AIAA-97-1141

Optimization of Stiffened Panels in which Mode Jumping is Accounted for

David Bushnell, Charles C. Rankin
Department H1-31, Building 255
Lockheed-Martin Palo Alto Research Laboratory
3251 Hanover St., Palo Alto, California 94304

Eduard Riks
Aerospace Engineering Department
Delft University of Technology
The Netherlands

ABSTRACT

PANDA2 is a computer program for the minimum weight design of stiffened composite, flat or cylindrical, perfect or imperfect panels and shells subject to multiple sets of combined in-plane loads, normal pressure, edge moments and temperature. STAGS is a general nonlinear finite element code that is specifically designed to analyze especially difficult stability problems in shell structures. Weight optimization of stiffened panels can be particularly troublesome when local buckling is allowed to occur in the pre-collapse state. For these systems, designs may be affected by interaction between local modes, a mechanism that manifests itself as mode jumping and is difficult to characterize. In this paper we describe how in PANDA2 mode jumping is detected and suppressed in optimized panels. Two axially compressed blade stiffened panels optimized by PANDA2 for service in the far postbuckling regime were numerically tested by STAGS. Mode jumping was permitted to occur below the design load in the first panel and suppressed in the second. Results obtained by STAGS are in reasonably good agreement with predictions by PANDA2. The first panel exhibits mode jumping well below the design load. Application of STAGS to this panel reveals that even though the mode jump involves little change in potential energy it generates large amplitude oscillating stresses with significant stress reversal that might well cause fatigue and delamination. The oscillating stresses are caused by postbuckling lobes moving to and fro along the panel axis immediately after initiation of the mode jump.

INTRODUCTION

The PANDA2 code[1,2,3] is a fast interactive computer program that provides the user with the optimum design of stiffened panels of various shapes and materials including composite fabrications. Because of the particular nature of this code with its simplifying assumptions and the inherent nonlinear behavior of locally postbuckled panels, the results must be checked thoroughly by either an experiment or by an analysis with an independent general-purpose finite element code (or both). In PANDA2 it is easy to check the results with the robust finite element code STAGS because PANDA2 automatically translates its output design into model input for STAGS [4,5]. The STAGS code can thus easily be used to check optimization designs that are produced by the PANDA2 user.

Weight optimization of stiffened panels designed for service in the local postbuckling regime can lead to a behavior dominated by mode interactions such as mode jumping[6,7,8,9] whereby the deformation state of the panel jumps from one mode shape to another as the load is increased. This phenomenon may or may not have a detrimental effect on the integrity of a panel, depending on the energy content of the jumps, on whether or not stresses oscillate significantly because of the jumps, and on the details of panel fabrication. For example, delamination in a composite panel can initiate or propagate as a result of mode jumps that release energy or otherwise alter the response significantly. Early fatigue failure might occur if the locations of maximum

stress oscillate during the mode jumping. Consequently, the designer might want to prevent serious mode jumping from occurring in his design. To provide this option, PANDA2 was equipped with a "prevent mode jump" constraint. We describe results of tests of this constraint here.

Until recently it was very difficult to use STAGS to analyze panels in which mode jumping occurs before failure. This behavior, which is transient, cannot be analyzed with the traditional static path-following technique that the STAGS code employs.[5] This difficulty has recently been overcome by judicial combination of the path-following technique and transient integration methods. Now it is possible to check PANDA2 designs that exhibit mode jumping in their load-deformation response[8,9]. A short description of the STAGS solution strategy is given.

The objectives of this paper are:

1. To describe how the results from PANDA2 and STAGS compare for a stiffened panel optimized by PANDA2. The panel is designed to carry loads far in excess of the local buckling load of the panel skin.

2. To describe and evaluate the constraint condition in PANDA2 that is supposed to prevent serious mode jumping before the design load is reached.

3. To demonstrate the capability of STAGS to obtain the nonlinear collapse load of panels in which mode jumping occurs at loads below the design load.

THE PANDA2 PROGRAM

PANDA2[1], which supersedes PANDA[2] but which contains many of the buckling algorithms from PANDA[3], finds minimum weight designs of laminated composite flat or curved cylindrical panels or cylindrical shells with stiffeners in one or two directions. Stiffeners can be blades, tees, angles, or hats. Truss-core sandwich panels[10] and stiffened sandwich panels with honeycomb or foam core[11] can also be handled, as well as isogrid-stiffened panels with added rings[12]. The panels or shells may have initial imperfections of the form of general, inter-ring, and local buckling modes[13]. The panels or shells can be loaded by as many as five combinations of in-plane loads, edge moments, normal pressure, and temperature. The material properties can be temperature-dependent. Local, inter-ring, and general buckling loads are calculated in PANDA2 with use of either closed-form expressions[3] or with use of discretized models[1] of panel cross sections. The discretized model is based on one-dimensional discretization similar to that used in the BOSOR4 computer code[14]. An analysis branch exists in which local post buckling of the panel skin is accounted for[15]. In this branch a constraint condition that prevents stiffener pop-off is introduced into the optimization calculations[1]. The postbuckling theory incorporated into PANDA2 is similar to that formulated by Koiter for panels loaded into the far-postbuckling regime [16].

PANDA2 can be run in five modes:

1. optimization,
2. simple analysis of a fixed design,
3. test simulation,
4. design sensitivity, and
5. load-interaction.

Optimization in PANDA2 is performed with use of the constraint-gradient-based ADS routines created by Vanderplaats and his colleagues[17,18]. There is a processor in the PANDA2 system called STAGSMODEL that automatically generates an input file for the STAGS computer program[19]. Thus, STAGS[4,5,20], which is a general purpose nonlinear finite element analyzer, can be used with reasonable ease to check the load-carrying capacity of stringer-stiffened panels optimized with PANDA2[19,21]

MODE JUMPING

It has long been known that the optimization of plates, stiffened panels and other thin-walled structural components designed to carry compressive loads may lead to a panel behavior that is governed by clustered bifurcation points or compound bifurcation points[22]. By clustered bifurcation points we mean that along the pre-buckling equilibrium curve of the panel under load, bifurcations occur at values of the load that are very close together, see Fig. 1. It is also well known that under such conditions the equilibrium branches of these bifurcation points are intertwined and display secondary bifurcations. Some of these branches have stable parts, but most of them are unstable. This may, in general, imply imperfection sensitivity because the bifurcations may have become unstable. Improperly formulated automated panel optimization may therefore lead to designs that fail long before the bifurcation load is reached, so that the computed design optimum does not in fact represent a feasible design[22].

With plates and stiffened panels that are only mildly curved in the transverse direction, the clustering sketched in Fig. 1 may still occur but it does not always lead to a direct lowering of the failure load. There are two subjects that have attracted attention in the literature which are associated with this clustering effect.

The first is called "mode interaction", defined as an interaction between a buckling mode of a long wave length with one or more modes of a short wavelength. Structures that exhibit mode interactions may be imperfection sensitive. They have been studied extensively in the literature[23,24,25].

The second subject is called "mode jumping", defined as interaction between mode shapes of short wave length and other so called "local modes"[6,7,26-30]. Structures that exhibit mode jumping (Stein's[6,7] is a perfect example) can be loaded above the initial buckling load as shown in Fig. 2a, in which stable equilibrium exists along branch *2* This initial stable postbuckling phase is followed by a loss of stability as soon as a secondary bifurcation point is reached. Further loading will then result in a dynamic departure from branch *2* to a neighboring stable equilibrium branch *3*. During this transient event the mode shape changes from its current postbuckling form into a different form that belongs to the new stable tertiary branch. This branch may or may not be (statically) connected to the previous branch from which the jump started. The precise situation will depend on the structural configuration and loading. Further loading along stable branch *3* may then end with another jump to yet another stable branch *4* and so on (see Fig. 2a).

The above description of the jumping behavior pertains to a panel that exhibits true bifurcation points along the primary loading path because its geometry is perfectly symmetric. In reality, panels are slightly imperfect so that a modification of the behavior will be observed. First of all, the transition into the first stable buckling mode will occur gradually, such as shown in Fig. 6 of [15]. When the load is further increased, a jump may occur but this will then most likely take place from a limit point rather than a bifurcation point [8]. Even though bifurcations in the branching diagram of a panel will usually disappear when it is imperfect, the overall behavior most often resembles what occurs in the perfect panel. However, the jumps will not always correspond to the same mode changes and may occur at different values of the load from those of the perfect panel.

The jumps that occur in the way just described may not have enough energy content to damage the panel severely if they occur infrequently during service. On the other hand, mode jumping always involves an abrupt change in postbuckling local mode shape. Therefore, the locations of the peak postbuckling bending stresses, which may be substantial, shift along the length of the panel. At a given material point the peak stresses may oscillate during a mode jump, not because the postbuckling deflection lobes oscillate in a manner analogous to a modal vibration, but because the lobes translate to and fro in the axial direction, a type of motion that can occur with only very small corresponding oscillation of the end shortening and therefore little change in potential energy. This phenomenon is exhibited in the examples provided here. If this happens repeatedly during service, fatigue could be a problem even if the energy content of the mode jump is low.

Experience with mode jumping indicates that the energy content of mode jumps increases with the jump number (with increasing load) to such a degree that irreparable damage may be sustained even on the first occurrence in service. Caution must be exercised when mode jumping is allowed in a design.

The analysis of a structure that exhibits such behavior is very demanding. In the literature there have been attempts to come to grips with some relatively simple examples of mode jumping, such as in an axially compressed plate strip[26-30]. Koiter's solution[31] for an infinitely long plate strip in compression for loads far in excess of the first bifurcation load serves as a constructive approximation to the mode jumping problem of a long plate.* Koiter's method determines the stationary value of the potential energy from a response constructed with mode shapes that have continuously variable wavelengths in the axial direction (varying with load, not with axial coordinate) and variable cross sections in the transverse direction.

In PANDA2 the axial wavelength of the postbuckling pattern is also allowed to vary continuously with

* This report[31] preceded the report[16]. The former is restricted to axial compression only. The latter represents an extension to the combination of axial compression and shear. Koiter's solution[31] can be seen as the solution of the mode jumping problem of a plate strip of infinite length where the changes in modeshape occur continuously with variation of the load. Koiter's work does not refer explicitly to the phenomenon of mode jumping.

increasing load in a manner similar to that described by Koiter[31]. Variation of postbuckling deformation over the panel cross section is achieved in PANDA2 by expansion of the postbuckling displacement field in a power series of the critical local bifurcation buckling mode[15].

In the studies[26-30] a perturbation technique is applied to construct parts of the branching diagram in the neighborhood of the first two bifurcation points, by means of which the jumping phenomenon can be explored. The practical significance of this approach is rather restrictive, however, because it is very difficult to apply the technique to structures with a more complex geometry. Even if one considers brute-force computational techniques, such as path-following methods[32-34] for the solution of the nonlinear equations generated by finite element models, a complete solution of the branching diagrams of such cases seems to be out of the question.

For the designer a knowledge of the complete branching diagram of a panel that exhibits mode jumping is fortunately not very useful because this diagram is extremely difficult to analyze, especially when the number of interacting modes is large. On the other hand, the possibility to compute the load-deformation path of a panel in space and time and thus to simulate both the static and dynamic behavior of the panel under slowly increasing load offers useful information because it provides the load vs. end shortening relation, a means to compute the energy content of the jumps, and the states of the structure for every load step of the static phases of the analysis and every time step of the transient phases of the analysis. This is now done in STAGS through use of a combination of static path-following techniques and transient methods [35,8,9] described briefly in the section entitled "SIMULATION OF MODE JUMPING IN STAGS". For a stiffened panel that exhibits mode jumping the load vs. end-shortening diagram is similar to that plotted in Fig. 2b.

THE MODE JUMP CONSTRAINT IN PANDA2

Constraints on the design generated via PANDA2 include local buckling of stiffener segments, rolling of stiffeners, local, inter-ring, and general buckling, maximum displacement under pressure, maximum tensile or compressive stress along the fibers and normal to the fibers in each lamina, and maximum in-plane shear stress in each lamina, with stresses computed including load-induced amplification of all of the components of the initial imperfection as well as significant local postbuckling deformation.

A mode jump constraint with the identifying phrase

"Hi-axial-wave post-post-buckling of panel skin"

has been introduced into PANDA2. This constraint can be turned OFF or ON by the user. The purpose of the "mode jump" constraint, which is modeled as a static (bifurcation) event in PANDA2, is to prevent serious dynamic mode jumping from occurring in panels optimally designed for service in the far-local-postbuckling regime. By "serious" is meant mode jumping at loads well in excess of the initial local bifurcation buckling load. In PANDA2 the "mode jump" constraint, even when turned ON by the user, is activated only if the applied load is at least twice the initial local buckling load.

The following computational steps are used in PANDA2 to generate the "mode jump" constraint for each design evaluation:

1. The critical (lowest) local buckling load factor and mode shape are generated for the discretized skin-stringer panel module as described in [1]. (An example of an undeformed and deformed discretized skin-stringer panel module is displayed in Fig. 10.)

2. The post-local-buckling equilibrium state of the panel is computed as described in detail in[15]. (See Figs. 10 and 11, for example).

3. The new distributions of the membrane stress resultants, N_x, N_y, N_{xy}, over the entire discretized cross section of the skin-stringer module are derived from the known post-local-buckled equilibrium state. The new distribution of N_x is qualitatively similar to that shown in Fig. 24 of [1]: N_x is greatly diminished midway between stringers and increased near and in the stringers. In Fig. 2a the stresses, N_x, N_y, N_{xy}, belong to the branch 2.

4. A "post-post" bifurcation buckling problem is set up and solved. This eigenvalue problem is entirely analogous to the initial local bifurcation buckling problem: Bifurcation buckling load factors are computed vs. number of axial halfwaves. However, in the "post-post" bifurcation buckling problem the new nonuniform distribution of N_x over the cross section of the panel module is used. *Local postbuckling*

deformations are ignored. The new search over the number of axial halfwaves is conducted starting from $M = 2m_{(crit)}$, where $m_{(crit)}$ is the critical number of halfwaves determined for initial local buckling. The "post-post" bifurcation buckling mode with number of axial halfwaves, $m^*_{crit} \approx 2m_{crit}$, in which m^*_{crit} is the number of axial halfwaves corresponding to the critical (lowest) "post-post" bifurcation buckling eigenvalue is the mode that determines initiation of transfer to Branch 3 in Fig. 2a or Branch 2 in Fig. 2b. The computation in PANDA2 corresponds to the determination of a bifurcation point in a fictitious prebuckling state of the panel in which the redistribution of N_x corresponding to the post buckling state at some point on Branch 2 in Fig. 2a is accounted for but buckling deflections are neglected. We hope that in this way we will obtain a good estimate of the load threshold beyond which a dynamic change in the number of axial halfwaves in the far post-locally-buckled state is likely. If this estimate is below the design load and significantly above the initial local buckling load we assume that "serious" mode jumping may take place, that is, the consequences for the structure may be dire.

5. Given the "post-post" buckling load factor, the "mode jump" margin is computed from the formula:

margin = ("post-post" buckling load factor)/(factor of safety) - 1.0

6. Gradients of the "mode jump" constraint with respect to small perturbations of each of the decision variables are computed, just as with all other "behavioral" constraints such as general buckling and stress. Then Vanderplaats' optimization routines [17] are called to generate a new design.

As with all behavioral constraints in PANDA2, the "mode jump" constraint is evaluated (for each design iteration or pass through the optimizer ADS) at the current design and at K neighboring (perturbed) designs in which K equals the number of decision variables in the problem. (In the rather simple case discussed in the section entitled "EXAMPLE" there are only three decision variables: height of the stringer, thickness of the panel skin, and thickness of the stringer.) The six steps outlined above (as well as any steps required to determine any other behavior, such as general instability and stress) are traversed many, many times before a final optimum design is achieved. For each design iteration, constraint gradients are established from the difference in behavior (e.g. buckling load factor) at the perturbed design and at the current (unperturbed) design. The amount by which each decision variable is perturbed depends on the maximum sensitivity of behavior to that perturbation.

PANDA2 uses certain short-cuts to obtain perturbed behavior corresponding to each perturbed design. For example, PANDA2 uses buckling modes corresponding to the unperturbed design as starting vectors for iterations to extract the critical eigenvalues and mode shapes for the perturbed designs.

One can appreciate that for more complex panels, such as a laminated composite panel with both stringers and rings and with possibly many load sets, one must resort to all sorts of approximations, short-cuts, and "tricks" to obtain reasonably accurate predictions with as few calculations as possible. It is admitted that the "mode jump" predictor used in PANDA2 is a crude one (especially since only the redistribution of N_x, N_y, N_{xy} in the post-local-buckling regime is accounted for, with the effect of local normal deflections ignored). Its effectiveness should be tested through extensive application of PANDA2 and STAGS.

THE STAGS PROGRAM

STAGS (Structural Analysis of General Shells), is a shell finite element program with a strong bias towards stability analysis capabilities[4,5,20]. Apart from having a good nonlinear shell modeling capability (small strain but arbitrarily large displacements and rotations), it is also equipped with path-following techniques that make it possible to solve stability problems such as bifurcation buckling and collapse. The modeling capabilities include many design features that are frequently encountered in lightweight structures in the field of aero- and astronautics: a whole range of stiffener models, shell wall materials including composites, etc. In addition to the solution techniques for computing the static equilibrium branches of these models, STAGS also possesses robust transient time stepping methods. It is the unique availability of a combination of advanced static and transient solution strategies that proves most effective in the cases where mode jumping plays a role. We will discuss these particular types of calculations in the following section.

SIMULATION OF MODE JUMPING IN STAGS

As follows from the discussion in the section entitled "MODE JUMPING", the phenomenon of mode jumping is simply a collapse or snap buckling event as described by the theory of elastic stability: a transient

change of deformation that occurs at a value of the load equal to or slightly in excess of the critical load that belongs to the bifurcation point or limit point. The only difference with the classical notion of collapse is that such a jump is not necessarily detrimental to the integrity of the structure. Damage depends on the frequency of occurrence during service of the structure, on the number and amplitude of stress oscillations precipitated by the jump and whether or not these oscillations involve stress reversal, and on the energy release associated with the jump, that is, the difference between the potential energy of the structure before and after the jump. In some plate structures for example the energy release can be so small that a series of successive jumps can perhaps be tolerated as the load increases up to and beyond a specified maximum (the design load).

According to the theory of elastic stability, collapse takes place at an unstable critical state of equilibrium [36,37,9]. Unstable critical points in general are either a proper limit point (A) or unstable bifurcation points (B,C) in Fig. 3. Before such a point is reached (when the load is still below the critical value) the equilibrium is stable. At such a state a small externally applied perturbation will be counteracted by the structure in such a way as to restore the perturbed state to the original equilibrium state. A stable equilibrium point is therefore called a point of attraction.

When an unstable critical state is exceeded the property of restorative reaction forces is impaired. At this point there may be one or more particular perturbations from the equilibrium state that will induce a repellent reaction in the structure. The repellent force works in the direction of these special perturbations and thus initiates a motion that is divergent. The motion that develops in this way will gain momentum at a rate that depends on the amount of potential energy freed and converted into kinetic energy. In the actual situation and also in our simulations this motion is resisted by damping. Therefore, if a stable post-jump static equilibrium state exists at the load level corresponding to mode jumping, the kinetic energy will eventually decay. The motion will subside at another attractor, a stable equilibrium state that acts as a new focus for the orbit that the motion follows, such as Branch *3* in Fig. 2a..

The special direction of the perturbation that will best initiate the transient motion from the unstable critical state turns out to be given by the *buckling mode* associated with this state in the following sense: the perturbation should point to the *unstable* branch *1* of the limit point (Fig. 3A) or the unstable branch *2* that goes through the bifurcation point [8,9] (Figs. 3B,C). Please note that this figure, as well as Figs. 1 and 2, represents a *projection* of the general solution in an $N+1$ dimensional space of displacement variables N and the load intensity factor λ, to a 1+1 dimensional space of one displacement component and the load factor λ. In Fig. 3 the direction of the displacement component is the buckling mode, the amplitude of which is denoted μ.

To make use of these findings, we adopted in [8,9] the following computational strategy. We first compute the fundamental state of the panel previously optimized by PANDA2 using the standard path-following technique available in STAGS [33]. In Fig. 3 this computation is symbolically indicated by the small open circles along the primary paths denoted by *1* (an open circle is a solution point). Critical points that are part of these paths betray themselves in various ways, for example through sign changes of the determinant of the stiffness matrix or changes in the number of negative entries on the main diagonal of the factored stiffness matrix. It is possible with a simple technique to determine the critical states with some accuracy[32-34], but this is not always required in the type of analysis that we consider here. The identification of the type of critical point, limit or bifurcation and stable or unstable, is more important.

In the case of a limit point the identification is trivial because in that case the load will reach and pass a maximum during the solution, an event that is easily monitored. In the case of a bifurcation point, the matter is slightly more complicated because a bifurcation point is a critical point that cannot in general be detected by observing the load factor. What usually happens is a change of sign in one or more of the diagonal terms of the factored stiffness matrix without a reversal of the sign of the path derivative of the load λ. However, to identify what type of bifurcation is encountered, we are required to conduct a calculation of the branch at the bifurcation point. This is possible in STAGS with the aid of a branch switch procedure[20]. Once small parts of the branches *2* in Fig. 3 are computed, we also know whether we have a unstable skew symmetric point (B) or an unstable symmetric point (C) or a stable symmetric point D.

After these preparations, we continue the analysis by computing the path that the actual structure follows. In the case of a stable symmetric point (D) the structure

will follow one of the stable branches *2*. The switch procedure mentioned earlier acts to initiate such a computation. In this case we continue with the static path-following procedure because the structure does not jump at such a state but instead follows a different stable equilibrium branch. There is a gradual change of the deformation with increasing load. This happens in one of the cases explored here.

More interesting are the unstable states B and C. To conduct a simulation of the transient buckling process that starts from these points, we use an implicit transient time stepping procedure called Park's method[38]. To start the computations in a way that is in agreement with what we know about the properties of the unstable points, we assume initial conditions as indicated in Fig. 3 by the solid points with arrows:

- In the case of the limit point (Fig. 3A), we start the time integration from an equilibrium point beyond the limit point by setting the load parameter to a value just above the limit load.

-In the case of the unstable bifurcation points B and C, we take a point computed earlier on the unstable (descending) branch as the initial condition with the load again adjusted to a value that slightly exceeds the critical load. This type of initialization will insure that the structure will enter the post-jump orbit[8,9] if a stable post-jump equilibrium state exists at that load level.

In most simulations of this sort the limit point is the most frequently encountered point of loss of stability. This means that we can set up the initialization with almost no effort. In the case of a bifurcation point the procedure described above is appropriate but it needs branch switching[20] in order to find the descending branch *2*.

Often we can avoid the branch-switching calculations after crossing a critical point by taking advantage of slight numerical round-off errors in solutions computed with standard path-following methods. These tiny errors represent perturbations from the actual equilibrium state that usually contain enough of the critical bifurcation buckling modal component to turn a transient solution toward the unstable buckling modal direction. This means that we can also try, with some confidence, to start from the unstable points on the primary branch *1* just above the critical load, with the expectation that the system will gain momentum as energy is released. Experience has shown that this approach almost always works, although it may take more time for the system to gain momentum as compared with the procedure sketched earlier. It is also very useful to add a small initial velocity proportional to the unstable mode, an option that is available in STAGS.

EXAMPLE

We present here a relatively simple example of a uniformly axially compressed, flat, blade-stiffened, steel panel that is optimized with PANDA2. Two alternative designs are produced: PANEL I with the mode jump constraint OFF, PANEL II with the mode jump constraint ON.

The two panel configurations thus obtained are then analyzed with STAGS to verify the reliability of the PANDA2 predictions.

-The PANDA2 Optimization and analysis-

Tables 1 and 2 provide the problem parameters and Figs. 4 - 14 display results from optimization and analysis of the optimized panel with PANDA2. The following boundary conditions are used: the panel is clamped at the two axially loaded ends. Wide-column behavior[1] is assumed, that is, the behavior of the entire stiffened panel is modeled with use of a single skin-stringer module[1] with symmetry conditions applied midway between stringers. In PANDA2 local buckling of the single module model is generated by forcing the normal displacement along one longitudinal edge to have the opposite sign from that along the opposite longitudinal edge (See Fig. 10).

Fig. 4 shows the evolution of the objective function (total panel weight) as a function of design iteration. For the first 15 design iterations the "mode jump" constraint "Hi-axial-wave post-post-buckling of panel skin" was turned OFF. That is, the panel was optimized without regard to the probability of mode jumping occurring at some load between the initial buckling load and the design load. At Iteration No. 15 the local buckling load factor is very close to $\lambda_c = 0.1$ (buckling load = 0.1 x 5000 = 500 lb/in). The optimum design at this point is called "PANEL I".

At Iteration No. 15 the "mode jump" constraint was turned ON, and design iterations were continued with "mode jump" turned on until convergence to a somewhat heavier optimum design was achieved at Iteration No. 29. This second optimum design is called "PANEL II". Note that the weight of the panel

increases significantly after the "mode jump" constraint is turned ON. The optimum weight with the "mode jump" constraint ON, 152 lbs., is about 20% higher than the optimum weight, 126 lbs., with the "mode jump" constraint turned OFF. Since this represents a considerable sacrifice, one must prove the necessity of turning ON the "mode jump" constraint. This is accomplished later by demonstrating via STAGS that significant oscillations of peak stresses (with stress reversals) occur during a mode jump in the optimized panel with the "mode jump" constraint turned OFF (PANEL I).

Figure 5 displays the evolution of all margins less than unity during all design iterations. (NOTE: margin = design constraint - 1.) It can be seen that at Iteration No. 15 the design margins presented in Table 3 are critical or close to critical. No "mode jump" constraint is listed there because it is still turned OFF. The "mode jump" constraint appears in Fig. 5 only between Iterations 15 - 29, after it has been turned ON by the user of PANDA2. For those iterations the "mode jump" constraint is critical and therefore affects the evolution of the design.

In Table 3 are listed three margins that all represent models of general instability, Margins 6, 10, and 14. Margin 6 is computed from a single discretized module model analogous to that shown in Fig. 22(b) of [1]. The wide column buckling mode resembles that shown in Fig. 22(c) of [1], that is, the skin-stringer cross section is permitted to deform in this representation of general buckling. (In Fig. 22 of [1] the panel is TEE-stiffened; here the panel is blade-stiffened.). Margin 10 is computed from a wide column model in which the stringers are smeared out and Donnell's theory is used to compute the general buckling load factor from the theory set forth in [3]. Margin 14 is computed from the same model as Margin 10 except that Sanders' theory is used [12] rather than Donnell's theory.

Figures 6 and 7 show the evolution of the design.The primary effect of turning ON of the "mode jump" constraint at Iteration No. 15 is to cause the thickness of the panel skin to increase.This results in the initial local bifurcation buckling load being increased to such a degree that the panel as loaded by the design load, N_x = -5000 lb/in, is no longer far enough into its locally postbuckled state for the redistribution of N_x over the module cross section to give rise to secondary bifurcation buckling (mode jumping) at a load below the design load.

Figures 8 - 14 show results obtained from PANDA2 used in the "test simulation" option, that is, an option in which the panel design is fixed and the applied axial load N_x is increased in steps. These results correspond to the optimized design at Iteration No. 15 (PANEL I: panel skin thickness = 0.057075 in.; stringer thickness = 0.16871 in.; stringer height = 1.6074 in.).

Figure 8 shows PANDA2's prediction of how the number of axial halfwaves in the local postbuckled pattern increases with N_x. PANDA2's treatment of number of axial halfwaves is similar to Koiter's[16,31]: the number of axial halfwaves computed in the postbuckling regime is permitted to vary continuously with load as if the panel were infinitely long. Details of how this is done in PANDA2 are given in [15]. The change in number of axial halfwaves from bifurcation (7 halfwaves in this case) to the design load, N_x = -5000 lb/in, (about 9.2 halfwaves in this case) is, of course, accounted for by PANDA2 during its computation of the stresses in the locally postbuckled panel. This predicted change in the number of axial halfwaves is in reasonably good agreement with STAGS results, as will be shown later.

Figure 9 shows how the membrane tangent stiffness components, $C_{11}^{tan}, C_{22}^{tan}, C_{33}^{tan}$, in the panel skin decrease in the local postbuckling regime. This decrease in skin tangent stiffness is, of course, accounted for in the computation of the 6 x 6 integrated constitutive matrix C_{ij} that governs overall buckling of the locally postbuckled panel. In this way the interaction of long and short wavelength buckling modes of the type discussed in [23-25] is accounted for in PANDA2.

NOTE: PANDA2 uses the postbuckled state only at the MIDLENGTH of the panel in the computation of the tangent stiffness components, $C_{11}^{tan}, C_{12}^{tan}, C_{22}^{tan}, C_{33}^{tan}$. This limitation has significant consequences in the case of PANEL I, as will be discussed later in connection with Fig. 32. It is emphasized that PANDA2 is based on a theory in which it is assumed that all local behavior, such as the postbuckled state, varies trigonometrically along the entire length of the panel with no axial modulation of the short wavelength postbuckled lobes as they interact with overall axial bowing of the panel.

Figure 10 displays the deformed PANEL I module cross section for five values of axial compression. The deflection is amplified by a factor of eight. In a test the actual deformed panel skin would probably not exhibit

the reversals in transverse curvature near the two longitudinal edges (midway between stringers: at abscissa coordinates 0 and 10 in Fig. 10) shown here for $abs(N_x)$ greater than 2000 lb/in. These reversals are doubtless a consequence of the limited expansion in PANDA2 of local postbuckling deflection in terms of local bifurcation buckling mode shape[15]. As written in Eq. (24) of [15] only two terms are used in this expansion, the linear and the cubic term. The consequence for design is not serious, it is thought, because the region of panel skin near the longitudinal planes of symmetry (midway between stringers) are under much less load in the far postbuckling regime than are the stringer and skin near the root of the stringer. Hence, critical stresses and strains are unlikely to occur in the region of panel skin where PANDA2's estimates of local postbuckling deflection are the least accurate.

Figure 11 shows a three-dimensional view of the local postbuckling deflection for a length of panel that spans one full axial wave of the post-local-buckling deflection pattern.

Figures 12 - 14 display axial, hoop (transverse to axial direction and in the plane of the panel skin), and in-plane shear strain components at the extreme fibers. The extremes of these values are later plotted in Figs. 26-28, which contain predictions from STAGS for PANEL I.

Note that up to Iteration No. 15 the "mode jump" constraint is turned OFF. Therefore, it is not included in the list of margins in Table 3 and of course does not affect the evolution of the optimum design up to Iteration No. 15. The design at Iteration No. 15 is judged by PANDA2 to be FEASIBLE because there are no significantly negative margins. (In PANDA2, designs are called FEASIBLE if all margins are greater than -0.01; designs are called ALMOST FEASIBLE if all margins are greater than -0.05; otherwise designs are called INFEASIBLE.)

After optimization with the "mode jump" constraint turned OFF, the PANDA2 user turns the "mode jump" constraint ON. At the zeroth iteration with the "mode jump" constraint ON (still at Iteration No. 15 in Figs. 4 - 7) the following margin is added to those just listed:

5 -3.19E-01 Hi-axial-wave post-post-buckling of panel skin -1; M=17 ; FS=1.0

The "mode jump" constraint is significantly negative. PANDA2 now rejects this design as INFEASIBLE because of the presence of this significantly negative margin. This margin is plotted in Fig. 5 starting at Iteration No. 15. Immediately after "mode jump" has been turned ON, PANDA2 finds that "post-post" bifurcation buckling occurs with $M = 17$ axial halfwaves and at a load factor of 1.0 - 0.319 = 0.681. Design iterations are continued from Iteration 15 through Iteration 29 with the "mode jump" constraint turned ON, leading to a new, considerably heavier optimum design at Iteration No. 29 with the margins listed in Table 4.

This new, heavier design has a local buckling load factor of approximately $\lambda_c = 0.19$ (axial load = 0.19 x 5000 = 950 lb/in), almost twice that of the optimum design obtained at Iteration No. 15 with "mode jump" turned OFF.

-The STAGS analysis-

In this section results from two STAGS analyses are reported:

1. a STAGS analysis of PANEL I, that is, the panel corresponding to the optimum design obtained with the mode jump constraint OFF (See Iteration No. 15 in Figs. 4, 6, 7). The values of the three decision variables at Iteration No. 15 are:

panel skin thickness	T(1) = 0.057075 in.
stringer thickness	T(2) = 0.16871 in.
stringer height	h = 1.6074 in.

2. a STAGS analysis of PANEL II, that is, the panel corresponding to the optimum design obtained with the mode jump constraint ON (See Iteration No. 29 in Figs. 4, 6, 7). The values of the three decision variables at Iteration No. 29 are:

panel skin thickness	T(1) = 0.075452 in.
stringer thickness	T(2) = 0.16256 in.
stringer height	h = 1.5896 in.

The STAGS finite element models are automatically generated with use of the PANDA2 data base via the PANDA2 processor called STAGSMODEL[19]. During execution of STAGSMODEL the user is prompted interactively for certain data. Among these prompts are the following two:

"Number of modules in the STAGS finite element model, NSTIF"

and

"Edges normal to screen (0) in-plane deformable; (1) rigid"

In the cases explored here the STAGSMODEL user's response to the "Number of modules..." prompt was "1". There is no anisotropy and no applied or Poisson-ratio-induced hoop resultant N_y nor in-plane shear resultant N_{xy}. The wide-column model is used to represent general instability. Therefore, a STAGS model with only a single module (one stringer with panel skin of width $b/2$ on each side of the stringer, where b = stringer spacing) is sufficient to predict with reasonable accuracy what happens when the panel of axial length 50 inches and transverse length 100 inches is uniformly axially compressed.

NOTE: In both the PANDA2 and the STAGS models it is assumed that the two axially loaded "clamped" ends of the panel are free to undergo Poisson-ratio transverse expansion under the axial compression. Therefore, no membrane hoop compression, N_y, builds up in the neighborhoods of the ends of the panel as the axial load is applied.

In all cases explored here except one the STAGSMODEL user's response to the "Edges normal to the screen..." prompt was "0". All of the results in this paper except those corresponding to Fig. 33 were obtained with the "in-plane deformable" option, which is felt to be the more conservative (leading to earlier failure of the panel according to STAGS). Fig. 47 of [19] shows a comparison of deformations, with use of both "1" (Fig. 47a) and "0" (Fig. 47b) in response to the "Edges normal..." prompt, for a panel with three modules under combined axial compression and in-plane shear. For an axially compressed panel with use of only a single module in the STAGS model, the "(0) in-plane deformable" option might lead to significantly larger maximum normal displacements in the panel skin in the far post buckling regime predicted by STAGS than those predicted by PANDA2, seen during a test of a multi-module specimen, or seen in the internal bays of a multi-module STAGS model, especially if the panel skin has a large Poisson ratio such as would be the case for a panel skin with an angle-ply laminate with layup angle, $\theta = [\pm 45]_n$. A multi-module STAGS finite element model would require much, much more computer time because there would be far more finite elements in the model and the bandwidth of the stiffness matrix would be far greater than it is in the single-module model.

The following sequence of STAGS runs is performed for the analysis of each structure, such as PANEL I and PANEL II:

1. The critical local bifurcation buckling mode and eigenvalue is first determined from linear theory. This is done in order to obtain an imperfection shape for the static nonlinear STAGS run to follow and to provide a comparison with PANDA2 predictions of local bifurcation buckling.

2. A STAGS nonlinear static run or a series of runs is executed in order to load the panel as far as possible without having to conduct any special transient runs to follow dynamic mode jumping behavior. A typical series of such STAGS runs is listed in Table 2 of [19].

3. A series of STAGS nonlinear dynamic runs is executed in order to follow mode jumping and possibly to achieve post-jump static equilibrium. Damping constants are used in these runs so that convergence will be achieved to a stable post-jump state if any such state exists. The load factor is held constant during this series of transient runs at a level two per cent higher than the highest load factor for which STAGS obtained a converged solution in the previous series of nonlinear static runs.

4. A STAGS nonlinear static run or series of runs is executed from the post-jump stable state up to the collapse load, or to the next mode jump if there is one.

The "410" finite element was used throughout the STAGS analyses reported here.

STAGS results for PANEL I

Figures 15 - 32 pertain to this subsection. Fig. 15 shows the local critical buckling mode of two single-module STAGS models: Model 1 has finite elements fairly uniform in size throughout. Model 2 has very narrow finite elements in the panel skin near the stringer and a more refined mesh on one side of the stringer than on the other. The purpose of Model 2 is primarily to capture with more accuracy the extreme fiber post-local-buckling hoop stresses in the panel skin adjacent to the blade. These high hoop bending stresses result from the large change in hoop curvature under the blade, especially evident in Fig. 10. As will be seen later these high hoop bending stresses oscillate immediately after the mode jump.

PANDA2 predicts local buckling with seven axial

halfwaves at a load factor close to 0.1. In the PANDA2 local buckling model the panel skin is assumed to be simply supported at the axially loaded ends even though the entire panel module (skin plus stringer) is clamped there. In the STAGS model the skin is clamped, except for transverse in-plane displacment v which allows Poisson-ratio expansion as mentioned previously. In-plane rotation of the stringer web is prevented. Allowing for these differences in boundary conditions in the PANDA2 and STAGS models, one sees that there is very good agreement between PANDA2 and STAGS for the buckling mode and load factor. (Also see Fig. 18a).

Figures 16 and 17 show the results of the first STAGS nonlinear static run on PANEL I with finite element Model 1. For this run a buckling modal imperfection amplitude of 0.005 inch was used. With use of nonlinear statics STAGS is unable to explore the region with load factor PA greater than 0.648 (Load Step 62). It appears that at a load factor of slightly more than 0.3 (Load Step 22) the panel experiences a gentle mode jump, that is, gentle enough that the Riks static path-following strategy can find equilibrium states for higher loads than the local peak at Load Step 22. The static solutions determined by STAGS beyond Load Step 62 appear to be on the same equilibrium curve as those covered between Load Step 42 and Load Step 62. It is therefore necessary to use the dynamic mode jumping strategy in order to determine the behavior of PANEL I for load factor, PA > 0.648.

The finite element Model 1 (Fig. 15a) was used to generate Fig. 18. Figure 18 displays edge-on views of the locally postbuckled PANEL I corresponding to five load steps during the initial static loading phase (a-e) and to the first static load step following the transient run and complete load relaxation (f). (Step 955 is the first static load step after the transient run for which the panel is in a state of static equilibrium. The load factor, PA = 0.6605 at Step 955). In Fig. 18 the amplitudes of the postbuckled normal displacements in the panel skin are the same in all six frames even though these frames correspond to different levels of applied load: a default option for deformation scaling, zero, was used in the input data required for the STAGS postprocessor, STAPL. This default causes the maximum displacement to be scaled to a certain fraction of the length of the undeformed structure. The purpose of this figure is not to demonstrate the growth or diminuation in the amplitude of the postbuckling deflection with changing applied load but rather to show how the number and position of axial halfwaves changes during loading.

Figure 18 contains several significant results:

1. Figure 18a demonstrates that the post-local-buckling mode from STAGS agrees well with that from PANDA2. While there are only six axial halfwaves along the length of the panel in the STAGS model rather than seven as predicted by PANDA2, the axial wavelength of each of the halfwaves is close to one seventh of the panel length. There are regions near the clamped ends in the STAGS model where there is small deflection because in the STAGS model the panel skin cannot rotate about a normal to the plane of the paper. This rotation constraint is absent in the PANDA2 model of local buckling and postbuckling of the panel skin, as mentioned previously.

2. From Fig. 18b we see that there are seven axial halfwaves along the length of the panel rather than six, as displayed in Fig. 18a. Hence there has been a mode "jump" (transition from one equilibrium branch to another) in the sense that the postbuckling state has changed in a non-proportional way between Load Step No. 10 and Load Step No. 22. The number of axial halfwaves has increased in spite of the fact that the applied load increases monotonically between Load Step No. 10 and Load Step No. 22, as shown in Fig. 17. This "gentle" transition is the stable type shown in Fig. 3D.

3. In Figs. 18(a-c) the postbuckling lobes on either side of the stringer are in phase with respect to axial variation. These states are in agreement with the PANDA2 model, which, being based on a "strip" method, requires in the absence of in-plane shear loading and anisotropy of the panel skin, that the postbuckling lobes on either side of the stringer always be in phase with eachother with respect to the axial coordinate because discretized deflections of the type shown in Fig. 10 are assumed to vary trigonometrically in the axial direction and the nodal lines of the postbuckling lobes have zero slope[15]. Note that in Figs. 18(d-f) the postbuckling lobes are out of phase in the STAGS model even though the panel skin is isotropic and there is no applied in-plane shear loading N_{xy}. This difference in the PANDA2 and STAGS predictions affects the predictions of stress and strain distributions and locations and values of maximum stresses and strains.

4. From Figs. 18b and 18c we see that as the panel unloads between Load Step No. 22 and Load Step No.

42 (Fig. 17), there appears one additional axial half wave in the postbuckled state. In an experiment on this panel a gentle dynamic "mode jump" would probably occur near the load factor corresponding to Load Step 22. We did not have to resort to a special transient STAGS run in this case because the static path-following technique was capable of tracking the changes in state of the panel during this presumably mild mode jump.

5. From Figs. 18(d,e) we see that the phase discrepancy between postbuckled lobes on either side of the stringer increases as the applied load increases. The number of axial halfwaves remains the same.

6. From Figs. 18(e,f) we see that during the many-stepped transient phase the number of axial halfwaves jumps from 8 to 10. The postbuckled lobes on either side of the stringer remain out of phase. (More details about the change in pattern of postbuckling lobes during the transient phase will be given later for PANEL I in connection with the finite element Model 2).

7. Fair agreement is obtained between PANDA2 and STAGS for prediction of the increase in the number of axial halfwaves as the panel is loaded into its far postbuckled state. (Compare Figs. 8 and 18).

Figure 19 displays results from a series of STAGS dynamic runs. The initial load at Load Step 63 is set at 1.02 x 0.648 = 0.6605, slightly above the equilibrium branching, as shown schematically in Fig. 3. At Load Step 950 the dynamic behavior is judged to have decayed enough to permit resumption of static loading.

In this case a single post-transient nonlinear static run was required to bring the applied load to within 99 per cent of the design load (PA = 0.99). At this point STAGS was unable to continue in a static mode. From results obtained via the STAGS postprocessor STAPL, we were able to determine that the panel was in the process of collapsing. Hence, no additional STAGS runs were made for this case.

Figure 20 shows the complete load-end-shortening curve for Model 1 of PANEL I. The transient phase occurs at a single load factor, PA = 0.6605. This load level agrees reasonably well with PANDA2's prediction of "post-post" bifurcation: "post-post" bifurcation buckling load factor = -0.319 + 1=0.681. (See Fig. 5, the curve labeled "Hi-axial-wave post-post buckling of skin"; at Iteration No. 15 the "mode jump" margin is equal to -0.319). For PANEL I, PANDA2 predicts collapse at a load factor of 1.1 rather than the 0.99 from STAGS. Later an explanation is offered for this discrepancy.

Figure 21 shows the growth of postbuckling deflections before the mode jump, and Fig. 22 shows the same after the mode jump. Comparison of Fig. 21(d) with Fig. 22(a) reveals that during the mode jump one additional full wave appears in the locally buckled panel. Figure 22b shows that the panel is collapsing in an overall bowing mode in which the stringer is on the convex side.

Figures 16-22 all correspond to PANEL I with use of the finite element Model 1 displayed in Figs. 15a, 21 and 22. Since Fig. 10 exhibits a rather concentrated hoop (transverse) bending of the panel skin in the immediate neighborhood of the stringer, we decided to use a more refined finite element model, especially for the panel skin segment under and near the stringer. This more refined finite element model of PANEL I, called Model 2, is depicted in Fig. 15b and in Fig. 23.

As can be seen from Fig. 23 the maximum effective stress at the load factor, PA = 0.6875, is predicted by the STAGS Model 2 of PANEL I to be about 140 ksi. This very high effective stress is concentrated in extremely small regions in the panel skin very near the stringer. With Model 1 the maximum effective stress depicted in an analogous plot is about 110 ksi. The reduction in the peak effective stress is mostly caused by an averaging of results over each element required by the STAGS postprocessor STAPL to generate fringe plots and partly caused by Model 1's inability to capture the steep change in postbuckling hoop curvature change of the panel skin in the immediate neighborhood of the stringer.

Note that the maximum effective stress in Model 2 of PANEL I at load factor PA = 0.6875 is very, very high (140 ksi). As listed in Table 1, the allowable effective stress was set in this case to a very high number: 1000 ksi. Therefore, the examples explored here are impractical in a strict engineering sense. The allowable effective stress was set very high in order to avoid active stress constraints from forcing the panel skin thickness to increase so that the "mode jump" constraint does not become active, or only becomes active very near the design load. Early attempts at setting up a good example for use in this study of mode jumping ran into this problem. We wanted a panel optimized by PANDA2 with the "stop modejump" constraint turned

OFF to exhibit serious mode jumping at a load considerably less than the design load. In order for this to happen the panel has to be optimized for service in the deep postbuckling regime. Very high local bending stresses are likely to occur in such panels. We therefore used the simple expedient of setting the allowable effective stress very high. We can, of course, still compare maximum stresses and strains obtained from PANDA2 and STAGS for this fictitious material. In future work on mode jumping, many, many examples, especially involving composite laminated panels, should be explored with use of realistic allowables for stress. Such a broad study is beyond the scope of this paper, which we regard as an introduction to optimization of panels in which mode jumping plays a significant role.

Figures 24 and 25 show the histories of the upper surface PANEL I skin hoop stress at the midlength of Model 1 (Fig. 24) and Model 2 (Fig. 25) in the finite element adjacent to the stringer where the maximum hoop stress occurs anywhere in the panel just before the transient phase of the analysis is initiated. With Model 1 the transient phase is conducted at a load factor, PA = 0.6605, and with Model 2 the transient phase is conducted at a load factor, PA = 0.7013. Both of these values of PA are two per cent above the maximum load factor for which STAGS was able to obtain a static solution. After correcting for the fact that the transient response phases of the STAGS analyses occur at slightly different load levels, we see from Figs. 24 and 25 that Model 2 predicts maximum hoop stress during the transient phase that is about 22 per cent higher than that that would be predicted with Model 1 at the same load level. Hence, the refinement in the finite element model is worthwhile.

It should be mentioned that in the initial static phase of the analysis the static path-following technique behaved quite differently for Models 1 and 2. With Model 1 a single static run was able to follow the the curve shown in Fig. 17 up to the maximum load factor, PA = 0.648, with use of only a single buckling modal initial imperfection, that shown in Fig. 15a. With Model 2 and use of the buckling modal initial imperfection shown in Fig. 15b, STAGS failed to obtain any static solution above a load factor of about 0.29. Before quitting at PA = 0.29, STAGS computed a buckling eigenvalue and eigenvector corresponding to the postbuckled state of the panel. The eigenvector, with an amplitude of 0.002 in., was used in addition to the original linear buckling mode shown in Fig. 15b as a new combined initial imperfection. Another static run was made starting from zero load. This time STAGS failed to find any static solution above a load factor of about 0.4. STAGS again computed a buckling mode at PA about 0.4, and this mode, with an amplitude of 0.0015, was added to the two previously determined buckling modes as a new combined initial imperfection. A final static run was then made from zero load. This time STAGS was able to follow the static equilibrium path, in 39 load steps, up to a load factor of 0.6875, at which point the transient phase of the analysis of Model 2 was initiated.

The technique of using multiple static nonlinear runs, accumulating with each failed run a new imperfection component or components and then starting over again at zero load, is described in Table 2, p 584 of [19]. This was the only way to entice STAGS to cover a complete load range in severely nonlinear and nearly singular systems before recent improvements [8,9].

Figures 26 - 28 show maximum strain components predicted from STAGS and PANDA2 for Model 2 of PANEL I. The PANDA2 points are read from Figs. 12-14. PANDA2 and STAGS agree well for maximum axial strain. For hoop strain and in-plane shear strain PANDA2 yields reasonably good agreement for load factors less than that for which the mode jump occurs. Beyond that STAGS predicts much more steeply increasing stresses with increasing load factor PA than does PANDA2. Most of the discrepancy is doubtless related to the fact that STAGS predicts a collapse load factor very close to 1.0 (Fig. 20), whereas PANDA2 predicts wide column buckling at a load factor very close to 1.1 (Margin No. 6 in Table 3). This discrepancy is explained later.

Fig. 29 is analogous to Fig. 18, except that Fig. 29 is based on finite element Model 2 rather than Model 1, and details of the change in postbuckling pattern are obtained only for the transient phase of computation. The six "snapshots" in Fig. 29 correspond to the six points indicated (a-f) in Fig. 30.

Each "snapshot" corresponds to a time for which the hoop stress plotted in Fig. 30 is at or near an extreme of its oscillation range. Careful inspection of the patterns in Fig. 29 reveals that what causes the oscillation of hoop stress plotted in Fig 30 are fairly small axial shifts in the buckling lobes. A given point anywhere along the panel length (except in the neighborhoods of the two ends) will "see" axial waves pass to and fro during the mode jump. The extreme fibers in the panel skin in the immediate neighborhood of the stringer will therefore experience alternate tension and compression in the

hoop direction as the panel wall flexes during these repeated axial translations of the postbuckling lobes.

This type of behavior might very well cause delaminations in a composite panel or fatigue in any panel. Because of this oscillating behavior of stress, with significant repeated stress reversals, we strongly recommend that optimum designs be obtained from PANDA2 with the "prevent mode jump" switch always turned ON.

Figure 31 displays the end shortening of Model 2 of PANEL I during the transient phase. Note that the transient behavior is associated with very little change in energy: there is very little transient axial motion at the end of the panel and hence very little dynamic work done by the applied axial load N_x, particularly for times greater than about 50 milliseconds. In spite of this, there are significant oscillations of maximum hoop stress throughout the time spanning the transient phase of the analysis (Fig. 30). Hence, it is felt that panels designed for service in the post-local-buckling regime should ALWAYS be optimized with the "stop modejump" switch turned ON in PANDA2.

For PANEL I, PANDA2 predicts collapse (wide column buckling: Margin No. 6 in Table 3) at a load factor of 1.1 [NOTE: (buckling load factor) = (FS)*(Margin+1) in which FS means "factor of safety"]. STAGS predicts collapse of PANEL I at a load factor very close to unity. It is felt that the 10 percent discrepancy is caused by the fact that PANDA2 uses the postbuckled state only at the MIDLENGTH of the panel to generate the distribution of effective axial stiffness over the cross section of the discretized panel module. This distribution of postbuckled axial stiffness is used for computation of the wide column buckling load factor. Figure 22b shows the deformation pattern in PANEL I predicted by STAGS very near collapse. A plan view of this deformation pattern appears as an insert in Fig. 32. Note that there is considerable sidesway of the blade near the clamped ends. This sidesway leads to a loss of effective axial stiffness of the blade, especially near the tip of the blade. The loss of effective axial stiffness in the blade leads to considerable reduction in the effective overall "EI" of the wide column near the clamped ends. This local loss of overall "EI" is of course "seen" by the STAGS model whereas it is not "seen" by the PANDA2 model. At the midlength of the panel the amplitude of blade sidesway is greatly reduced because the panel bows in a direction such that the tip of the blade is under less axial compression than the root of the blade. Since PANDA2 uses the blade sidesway at the midlength of the panel in its computation of postbuckled effective axial stiffness, it yields a higher wide column buckling load factor than does STAGS.

Figure 32 shows axial bowing as predicted by PANDA2 and STAGS. The theory used by PANDA2 is explained in ITEM 82 of [39]. Axial bowing as predicted by STAGS increases very steeply for load factor, PA > 0.85, presumably because of the reduction in effective overall "EI" near the panel ends as discussed in the previous paragraph. This difference in prediction of overall behavior of PANEL I for loads approaching the design load, PA = 1.0, doubtless accounts for the differing steepnesses of the curves from PANDA2 and STAGS for hoop and in-plane shear strain with increasing axial load plotted in Figs. 27 and 28, respectively. Fortunately, this type of discrepancy seems to occur only for panels loaded very far into the postbuckling regime. As will be seen later, a similar discrepancy in results between PANDA2 and STAGS does not exist for the panel optimized with the "prevent mode jump" constraint turned ON.

PANEL I was investigated again with use of STAGS. This time Lagrange constraints were introduced into the STAGS model that force the in-plane transverse displacement component v to vary linearly from one end of the panel to the other along the two unloaded (longitudinal) edges. This "straight-edges" model requires much more computer time than the model in which in-plane warping of the longitudinal edges is permitted because the bandwidth of the stiffness matrix increases from 144 to 364 for finite element Model 2. The load-end-shortening curve displayed in Fig. 33 requires about 20 hours on a DEC-ALPHA, half of that time spent for execution of about 700 time steps during the transient phase of computations. STAGS was able to track the static equilibrium curve up to a load factor, PA = 0.934 in a single run. The collapse load predicted with the "straight-edges" STAGS model is within one per cent of that predicted with the the earlier models in which in-plane edge warping was permitted.

STAGS Results for PANEL II

Figures 34 - 40 pertain to this section. PANEL II has dimensions corresponding to Iteration No. 29 in Figs. 6 and 7. This is the optimum design derived by PANDA2 with the "stop modejump" switch turned ON: panel skin thickness = 0.075452 in.; stringer thickness = 0.16256 in.; stringer height = 1.5896 in.

Figure 34 is analogous to Fig. 20. PANDA2 predicts mode jumping to occur at the design load, PA = 1.0 (Table 4, Margin No. 3). In the STAGS model an initial buckling modal imperfection amplitude of 0.007 in. was used. The imperfection shape is similar to those shown for PANEL I in Figs. 15a,b, except there is one less axial halfwave. Both PANDA2 and STAGS yield a linear bifurcation buckling load factor, PA = 0.19, for local buckling. In the initial nonlinear static run, STAGS was able to track the equilibrium curve to a load factor, PA = 1.094, well above the design load, PA = 1.0. Both PANDA2 and STAGS predict collapse of the panel at load factors close to 1.1, with PANDA2's prediction being the more conservative.

Figures 35 - 39 are analogous to Figs. 26 - 28. Two figures for each of hoop strain and in-plane shear strain are given because the location of maximum strain shifts along the length of the panel during the initial nonlinear calculations of static equilibrium. There is a "phase shift" of postbuckled lobes on either side of the stiffener as observed with PANEL I (Fig.18(a-e)). This "phase shift" is especially noticeable in Fig. 40.

Figure 40(a) depicts a distribution of upper surface hoop stress that very much resembles what one might expect from the postbuckling panel module deformation depicted in Fig. 10. for an isotropic panel with no in-plane shear loading. Because of the discontinuity in hoop curvature on either side of the stringer, which applies a line moment to the panel skin, there are equal and opposite hoop surface stresses in the panel skin on either side of the root of the stringer. These stress concentrations show up clearly along the midwidth of the STAGS model depicted in Fig. 40a. At the highest load attained in the nonlinear static analysis the postbuckled lobes on either side of the stringer have shifted in the axial direction relative to eachother so that the maximum compressive hoop stress now appears at the midlength of the panel. This maximum compressive hoop stress occurs on both sides of the stringer: there appears to be little discontinuity there, in sharp contrast to the state depicted in Fig. 40a. As mentioned previously, it is beyond the ability of PANDA2 to predict this kind of axial "phase shifting" behavior of the postbuckled lobes on either side of the stringer in the absence of anisotropy or applied in-plane shear loading.

From Figs. 40(c,d) it is seen that the distribution of in-plane shear stress in the panel skin, originally symmetric with respect to the midwidth of the panel module (Fig. 40c: the extreme fiber shear stress is symmetric because the normal displacements are antisymmetric, as shown in Fig. 10), becomes skewed as the load is increased (Fig. 40d). The maximum in-plane shear stress becomes much more concentrated in the far postbuckling regime. One can appreciate especially from Fig. 40d that, if mode jumps cause oscillatory axial shifting of the postbuckled lobes, significant cyclic extreme fiber stresses will occur at given material points in the structure. Again it is emphasized that panels should therefore be designed to avoid mode jumping, that is, with the "stop modejump" switch turned ON in PANDA2.

CONCLUSIONS

In the foregoing we discussed a new feature in PANDA2 that makes it possible to prevent serious mode jumping from occurring in panels that are designed to function in the locally post-buckled state. Because PANDA2 uses a mode jump constraint that is based on a heuristic argument, it remains necessary to check optimum designs generated by PANDA2 with an analysis that is based on a more refined computational model such as provided by the finite element code STAGS. The method of conducting such an analysis is described in this paper.

The following conclusions are drawn from the results presented here, which are all obtained for a uniformly axially compressed, blade-stiffened steel panel with maximum stress constraints neglected:

1. PANDA2's model for the initiation of mode jumping is reasonably well confirmed by STAGS results for panels optimized by PANDA2:

   a. with the "prevent mode jump" switch turned OFF, that is, with mode jumping ignored during optimization, and

   b. with the "prevent mode jump" switch turned ON, that is, with a constraint condition that prevents mode jumping from occurring at a load below the design load.

2. Mode jumps, even if associated with very small changes in potential energy, can generate high-amplitude oscillations of stress components with significant stress reversals, especially the extreme fiber hoop stresses in the panel skin adjacent to the stringer. This oscillation might well cause fatigue failures and delaminations. Therefore, it is strongly recommended that the "prevent mode jump" switch always be turned

ON during optimization with PANDA2.

3. The agreement between PANDA2 and STAGS for maximum extreme fiber strain in the far postbuckling range is acceptable for the purpose of preliminary design. PANDA2's predictions appear to be conservative provided that the load factor is not too close to the collapse load. We expect this will almost always be the case provided that the user turns the "prevent mode jump" switch ON before optimizing a panel.

4. Changes in the number of axial halfwaves in the locally postbuckled state can take place under monotonically increasing axial load.

5. The postbuckled lobes can shift by different amounts on either side of the stiffener even if the panel is isotropic and not subjected to any applied in-pane shear load. This phenomenon cannot be predicted by PANDA2. The differential axial shifting of course affects the locations of maximum stress and strain and probably their values.

6. Prevention of in-plane warping of the two longitudinal (unloaded) edges of the panel greatly increases the computer time required to explore a case but has little influence on the collapse load of the panel. in the one case explored here.

7. A very refined finite element mesh is required in the panel skin in the neighborhood of the root of the stringer in order to capture steeply varying extreme fiber hoop stresses there.

8. Optimization with the "prevent mode jump" switch turned ON leads to panels that are approximately 20 percent heavier than those optimized ignoring mode jumping. The collapse loads of the heavier, safer panels as computed from STAGS and PANDA2 are in very good agreement.

SUGGESTIONS FOR FURTHER WORK

1. Additional results of a similar kind should be obtained for laminated composite panels. Realistic stress allowables should be used.

2. Cylindrical panels should be investigated.

3. Cases should be explored with initial buckling modal imperfections included in the PANDA2 models.

ACKNOWLEDGMENTS

The authors first wish to acknowledge the long-term contributions of Mr. Frank Brogan, a principal developer of the STAGS computer program since its infancy in the early 1960's. D. Bushnell wishes to express his appreciation for the continuing support of Dr. Ron Dotson and Mr. Bill Sable, Spacecraft Analysis Department (Dept. E4-20) in Lockheed-Martin Missiles and Space Satellite Systems Division. Dr. Charles Rankin and Professor Eduard Riks appreciate the sponsorship over many years of Dr. James Starnes, Jr, Head of the Structural Mechanics Branch of the NASA Langley Research Center, for the continuing development of advanced nonlinear methods as introduced into STAGS. Mr. Bill Bushnell wrote the software, PLOTPS, that generated all of the "x-y" plots in this paper. He also helped the authors provide the proper format of the paper for the AIAA and continues to support D. Bushnell in the maintenance of the PANDA2 computer program on several UNIX-based workstations. Bo Stehlin is one of the creators of the STAPL program, by means of which the plots of deformed panels and the fringe plots of stresses were generated.

REFERENCES

[1] Bushnell D., "PANDA2 - Program for minimum weight design of stiffened, composite, locally buckled panels," Computers and Structures, 25, 469-605, (1987).

[2] Bushnell, D., "PANDA - Interactive program for minimum weight design of stiffened cylindrical panels and shells", Computers and Structures, Vol. 16, pp. 167-185, 1983

[3] Bushnell, D., "Theoretical basis of the PANDA computer program for preliminary design of stiffened panels under combined in-plane loads," Computers and Structures, Vol. 27, No. 4, pp. 541-563 (1987)

[4] Almroth B. O. and Brogan F. A., "The STAGS Computer Code", NASA CR-2950, NASA Langley Research Center, Hampton, VA (1978).

[5] Rankin C. C., Stehlin P., and Brogan F. A., "Enhancements to the STAGS computer code". NASA CR 4000, NASA Langley Research Center, Hampton, VA., (1986).

[6] Stein M., "The Phenomenon of Change of Buckling

Patterns in Elastic Structures", NASA Technical report R-39, National Aeronautics and Space Administration, (1959).

[7] Stein M., "Loads and Deformations of Buckled Rectangular Plates", NASA Technical Report R- 40, National Aeronautics and Space Administration, (1959).

[8] Riks, E., Rankin C. C., Brogan F. A., "On the solution of mode jumping phenomena in thin walled shell structures", First ASCE/ASM/SES Mechanics Conference, Charlottesville, VA, June 6-9, 1993, in: Computer Methods in Applied Mechanics and Engineering, Vol.136, (1996).

[9] Riks E.and Rankin C.C., "Computer Simulation of the Buckling Behavior of Thin Shells Under Quasi Static Loads", Archives of Computational Mechanics, to appear.

[10] Bushnell, D., "Truss-core sandwich design via PANDA2", Computers and Structures, Vol. 44, No. 5, pp. 1091-1119 (1992)

[11] Bushnell, D., "Optimum design via PANDA2 of composite sandwich panels with honeycomb or foam cores", 38th SDM Conference, April (1997).

[12] Bushnell, D., "Recent enhancements to PANDA2, " 37th AIAA Structures, Structural Dynamics and Materials Conference, April, 1996. Submitted to Finite Elements in Analysis and Design (1997).

[13] Bushnell, D. and Bushnell, W. D.,"Approximate method for the optimum design of ring and stringer stiffened cylindrical panels and shells with local, inter-ring, and general buckling modal imperfections", Computers and Structures, Vol. 59, No. 3, pp. 489-527 (1996)

[14] D. Bushnell, "BOSOR4: Program for stress, buckling, and vibration of complex shells of revolution," Structural Mechanics Software Series - Vol. 1, (N. Perrone and W. Pilkey, editors), University Press of Virginia, Charlottesville, 1977, pp. 11-131. See also Computers and Structures, Vol. 4, (1974) pp. 399-435; AIAA J, Vol. 9, No. 10, (1971) pp. 2004-2013; Structural Analysis Systems, Vol. 2, A. Niku-Lari, editor, Pergamon Press, Oxford, 1986, pp. 25-54, and Computers and Structures, 18, (3), (1984) pp. 471-536.

[15] Bushnell, D., "Optimization of composite, stiffened, imperfect panels under combined loads for service in the postbuckling regime", Computer Methods in Applied Mechanics and Engineering, Vol. 103, pp. 43-114 (1993)

[16] Koiter W.T., "Het schuifplooiveld by grote overschrijdingen van de knikspanning", ("The shear buckling mode at loads far above the critical value"), National Aerospace Laboratory, The Netherlands, Report X295, (1946).

[17] Vanderplaats, G. N., "ADS--a FORTRAN program for automated design synthesis, Version 2.01", Engineering Design Optimization, Inc, Santa Barbara, CA, January, 1987

[18] Vanderplaats, G. N. and Sugimoto, H., "A general-purpose optimization program for engineering design", Computers and Structures, Vol. 24, pp. 13-21, 1986

[19] Bushnell, D. and Bushnell, W. D., "Minimum-weight design of a stiffened panel via PANDA2 and evaluation of the optimized panel via STAGS", Computers and Structures, Vol. 50, no. 4, p569-602 (1994)

[20] Rankin, C. C., and Brogan, F. A., "Application of the Thurston Bifurcation Solution Strategy to Problems with Modal Interaction," AIAA Paper No. 88-2286 in Proceedings of the 29th Structures, Structural Dynamics, and Materials Conference Part 1 (1988), pp. 590--595.

[21] Bushnell, D. and Bushnell, W. D., "Optimum design of composite stiffened panels under combined loading", Computers and Structures, Vol. 55, No. 5, pp. 819-856 (1995)

[22] Thompson J.M.T., Hunt G.W., A General Theory of Elastic Stability, John Wiley & Sons, Ltd., (1973).

[23]. Tvergaard V., "The Sensitivity of a Wide Integrally Stiffened Panel under Compression," Int. Journ. Solids and Structures, Vol.9, 177 - 192 (1973).

[24]. Koiter W.T., Pignataro M., "A general Theory for the Interaction of Local and Overall Buckling of stiffened panels," WTHD 83, Department of Applied Mechanics, Technical University Delft, (1976).

[25]. Van der Neut A. "Mode Interaction with

Stiffened Panels", Proc. IUTAM Symposium on Buckling of Structures, Harvard University, (1974), 117 - 132. Springer Verlag (1976).

[26]. Supple W. J. "Changes of Wave-Form of Plates in the Post-Buckling Range", Int. J. Solids Structures, Vol., pp. 1243-1258, (1970).

[27]. Nakamura T. Uetani K. "The Secondary Buckling and Post-Buckling Behaviours of Rectangular Plates", Int. J. Mech. Sci., Vol., pp. 265-286, (1979).

[28]. Schaeffer, D. and Golubitsky, M., "Boundary Conditions and Mode Jumping in the Buckling of a Rectangular Plate", Communications in Mathematical Physics, Vol. 69, pp. 209 - 236 (1979).

[29]. Golubitsky, M. and Schaeffer, D., "Singularities and Groups in Bifurcation Theory", Volume I, Applied Mathematical Sciences, Springer Verlag, New York, Heidelberg, Tokyo, (1985).

[30]. Suchy H., Troger H. and Weiss R. "A Numerical Study of Mode Jumping of Rectangular Plates", ZAMM Z. Angew.Math. u. Mech., Vol. 65, 2, pp. 71-78, (1985).

[31] Koiter W.T., "De meedragende breedte bij grote overschrijdingen van de knikspanning voor verschillende inklemmingen van de plaatranden," ("The equivalent width at loads far above the buckling load for various boundary conditions along the plate edges"), NLL report 287, National aerospace Laboratory, (1943).

[32] Riks E., "Some Computational Aspects of the Stability Analysis of Nonlinear Structures", Comp. Meth. in Appl. Mech. in Engrg. Vol. 47 , 219-259, (1984)

[33] Riks E., "Progress in Collapse Analysis", Journal of Pressure Vessel Technology, Vol. 109/27 - 41, Febr..(1987).

[34] Seydel R., "From Equilibrium to Chaos, Practical Stability Analysis", Elsevier, New York-Amsterdam-London, ISBN 0-444-01250-8, (1989).

[35] Riks E., Brogan, F. A. and Rankin C. C., "Aspects of the stability analysis of shells, Static and Dynamic Stability of Shells" (W. B. Kratzig and E. Onate, editors), Springer Series in Computational Mechanics, Springer Verlag, Heidelberg (1990).

[36] Koiter, W.T., "On the Stability of Elastic Equilibrium", H.J. Paris Publ., Amsterdam (1945), English translation: Report nr. AFFDL-TR-70-25, Air Force Flight Dynamics Lab., Wright Patterson AFB, OHIO, (1970).

[37] Koiter W.T., "Elastic Stability and Post-Buckling Behavior," Proc. Symposium on Nonlinear Problems, (R.E. Langer Ed.), Univ. of Wisconsin Press, p. 257, (1963).

[38] Park, K.C., "An Improved Stiffly Stable Method for the Direct Integration of Nonlinear Structural Dynamics," J. Appl Mech. Vol. 42, pp 464-470 (1975).

[39] Bushnell, D., .../panda2/doc/panda2.news, a continually updated file distributed with PANDA2 that contains a log of all significant modifications to PANDA2 from 1987 through the present.

Table 1
INITIAL PANEL DIMENSIONS, MATERIAL PROPERTIES, AND LOADING

Axial length of panel	L = 50.0 in.
Transverse length of panel	B = 100.0 in.
stiffener spacing,	b = 10.0 in. (fixed in this example)
Initial height of stiffener,	h = 2.0 in. (decision variable)
Initial thickness of panel skin	t_1 = 0.1 in. (decision variable)
Initial thickness of blade	t_2 = 0.2 in. (decision variable)
Young's modulus	$E = 30x10^6$ psi
Poisson's ratio	$\nu = 0.3$
Allowable effective stress	$1x10^6$ psi
Weight density of material	$\rho = 0.3$ lb/in^3
Applied axial load (the design load)	N_x =-5000.0 lb/in

Table 2
MARGINS OF SAFETY FOR PANEL DESIGN

Local buckling	F.S. = 0.1 (local buckling permitted)
Wide column and general buckling	F.S. = 1.1
Effective stress	F.S. = 1.0

Table 3
MARGINS FOR OPTIMUM DESIGN AT ITERATION NO. 15 ("mode jump" turned OFF)

NO	VALUE	DEFINITION
1	1.58E-02	Local buckling from discrete model-1., M = 7 axial halfwaves; FS = 0.1
2	-1.30E-04	Local buckling from Koiter theory, M = 7 axial halfwaves; FS = 0.1
6	4.90E-03	(Wide column panel buckling load factor)/(F.S.) -1; FS = 1.1
7	-1.56E-03	(m=1 lateral-torsional buckling load factor)/(F.S.) -1; FS=1.1
10	1.80E-01	buck.(DONL); clamped general buck; M = 1;N = 1; slope=0.; FS = 1.1
14	1.80E-01	buck.(SANDERS); clamped general buck; M = 1;N = 1;slope=0.;FS = 1.1

Table 4
MARGINS FOR OPTIMUM DESIGN AT ITERATION NO. 29 ("mode jump" turned ON)

MAR. NO.	MARGIN VALUE	DEFINITION
1	9.13E-01	Local buckling from discrete model-1., M=6 axial halfwaves; FS = 0.1
2	8.95E-01	Local buckling from Koiter theory, M=6 axial halfwaves; FS = 0.1
3	-2.70E-03	Hi-axial-wave post-post-buckling of panel skin -1; M=12 ; FS = 1.0
4	5.24E-03	(Wide column panel buckling load factor)/(F.S.) -1; FS = 1.1
5	2.68E-01	(m=1 lateral-torsional buckling load factor)/(F.S.)-1; FS = 1.1
7	1.31E-01	buck.(DONL); clamped general buck; M=1; N=1; slope=0.; FS = 1.1
9	1.31E-01	buck.(SAND); clamped general buck; M=1; N=1; slope=0.; FS = 1.1

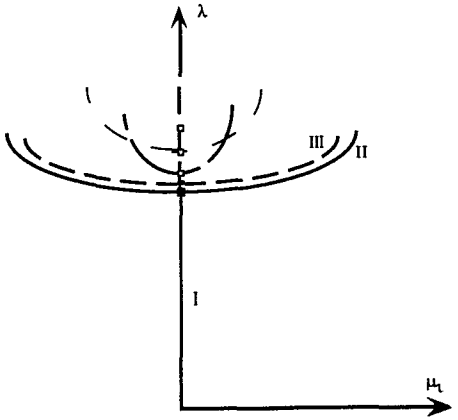

Fig. 1 Clustered bifurcation points

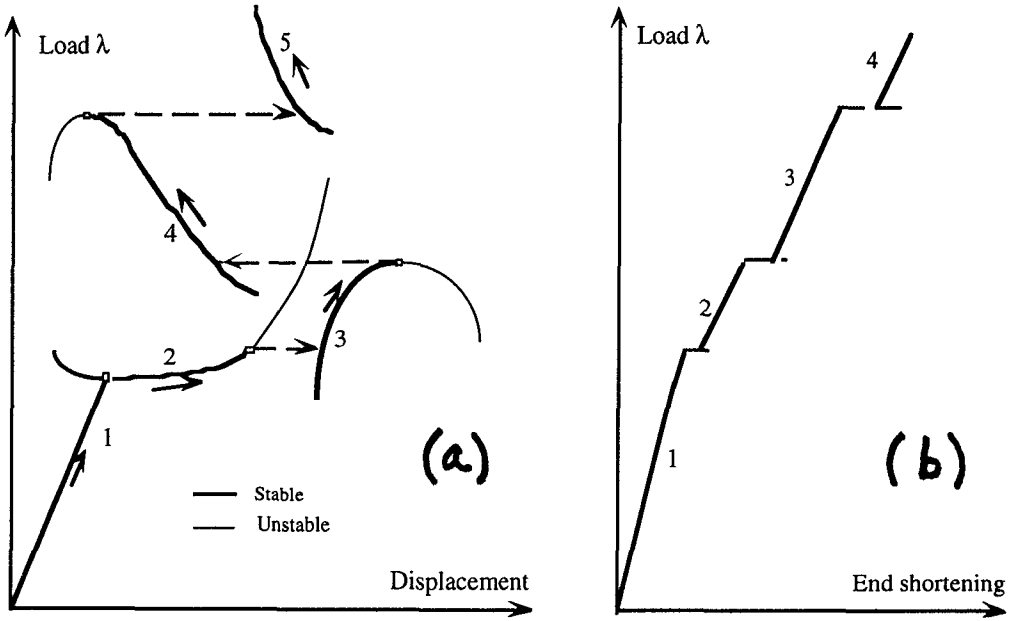

Fig. 2 (a) Mode jumping in general; (b) in axially compressed panels

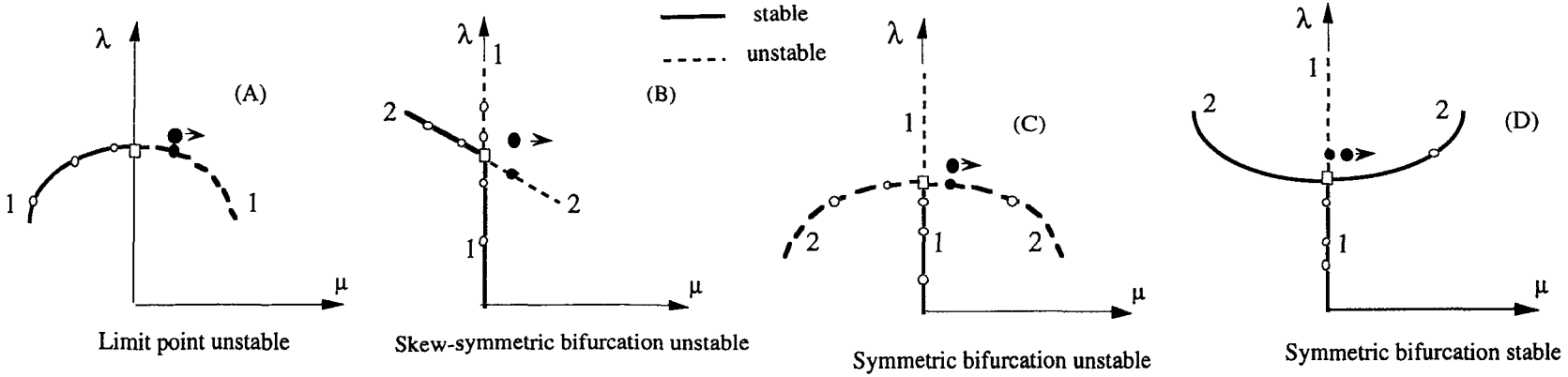

Fig. 3 Types of branching and initial conditions in STAGS for mode jumping

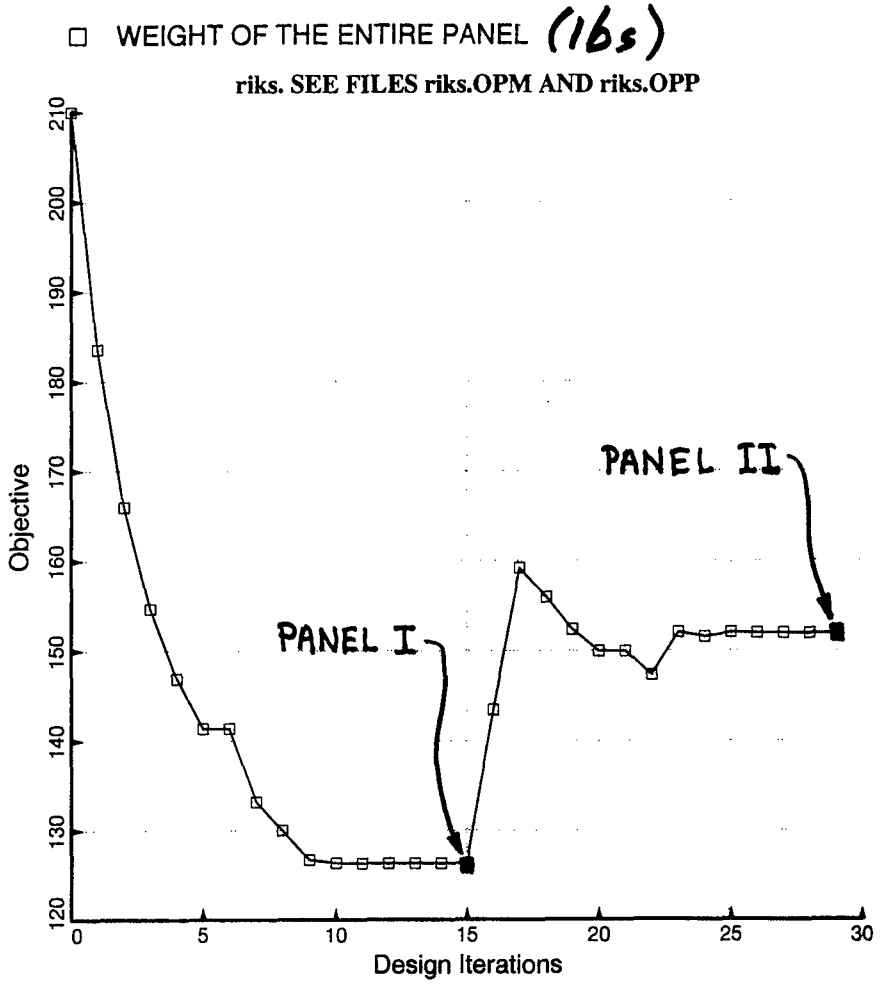

Fig. 4 Optimization in PANDA2 with "stop modejump" first turned OFF (Iterations 1 - 15), then turned ON (Iterations 15 - 29)

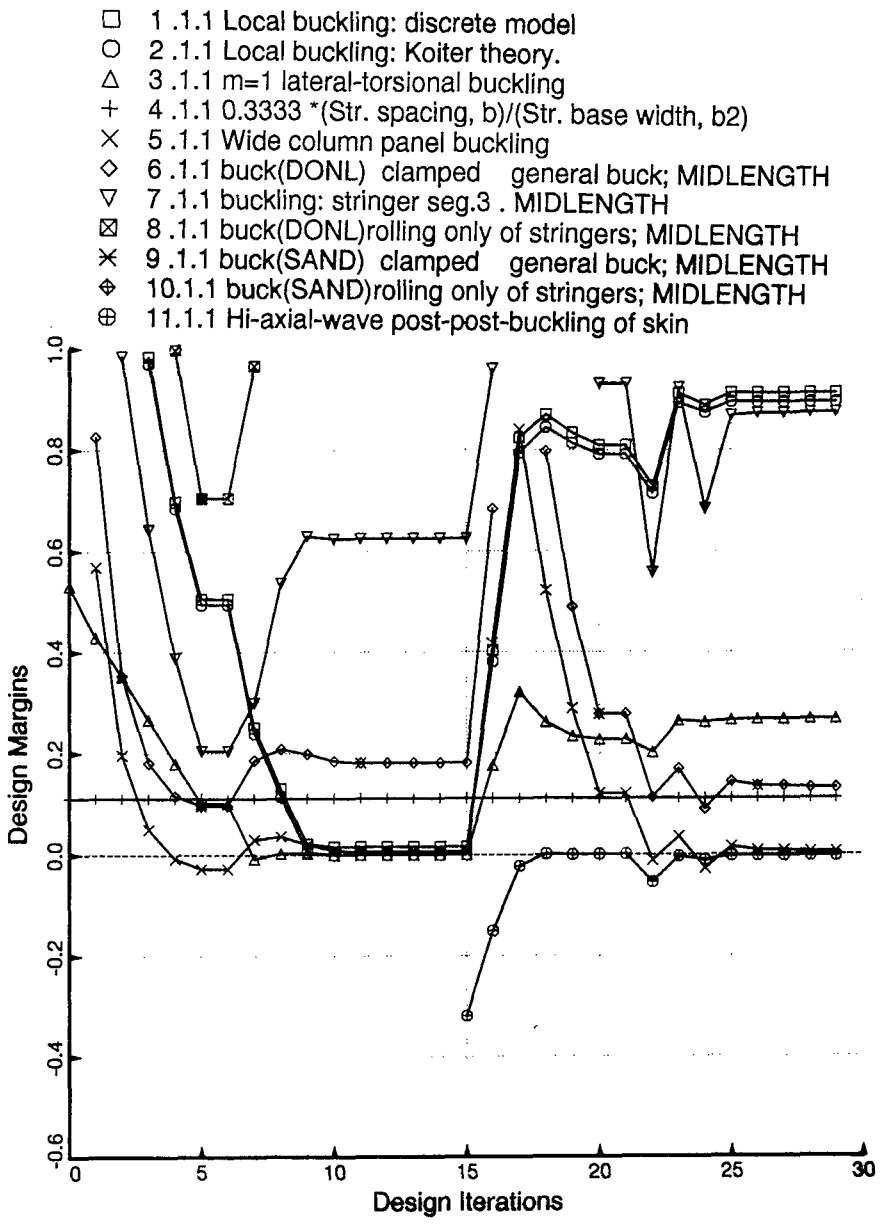

Fig. 5 Design margins during optimization with "stop modejump" first OFF, then ON

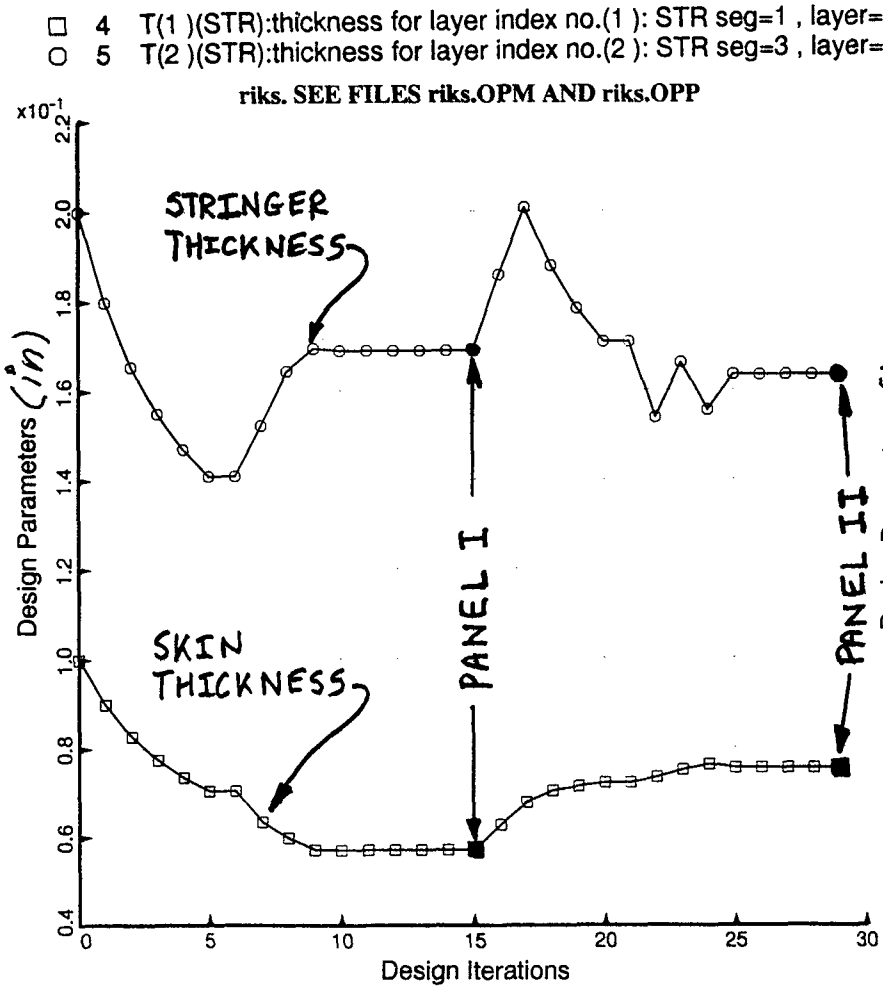

Fig. 6 Evolution of thicknesses with the "stop" modejump" constraint first turned OFF (Iterations 1-15), then ON (Iter. 15-29)

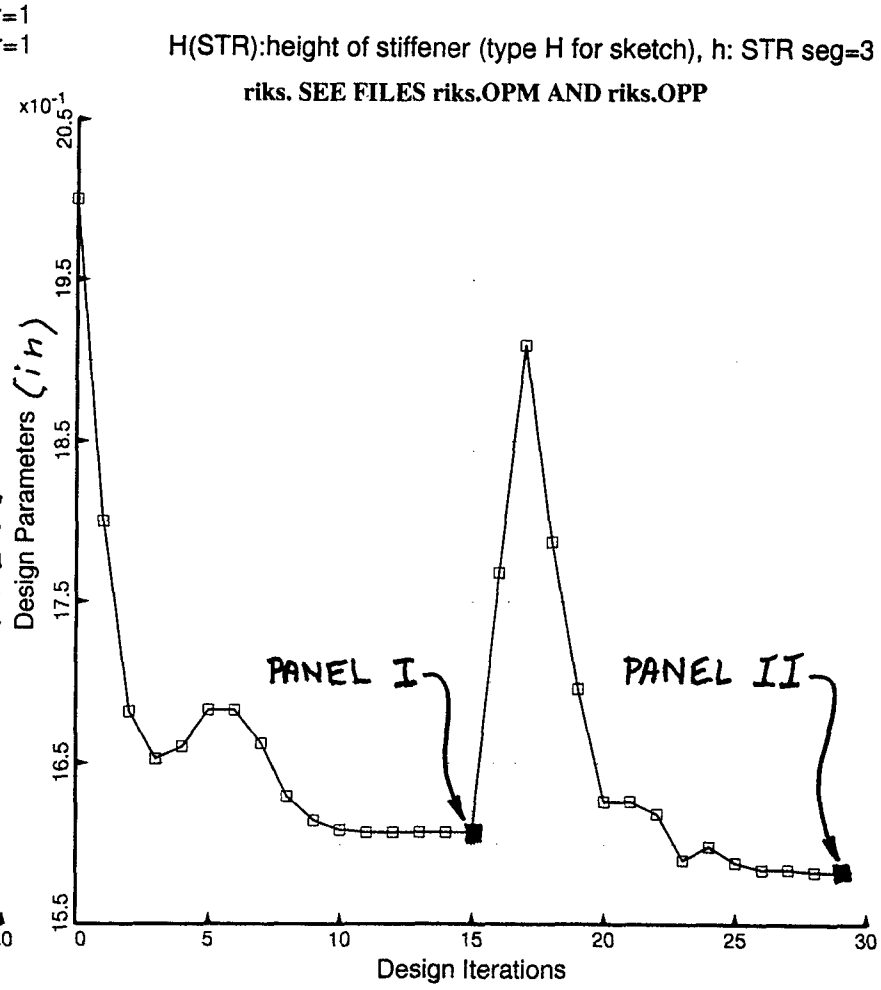

Fig. 7 Evolution of stringer height with the "stop modejump" constraint first turned OFF, then ON. The designs labelled PANEL I and PANEL II are analyzed with STAGS

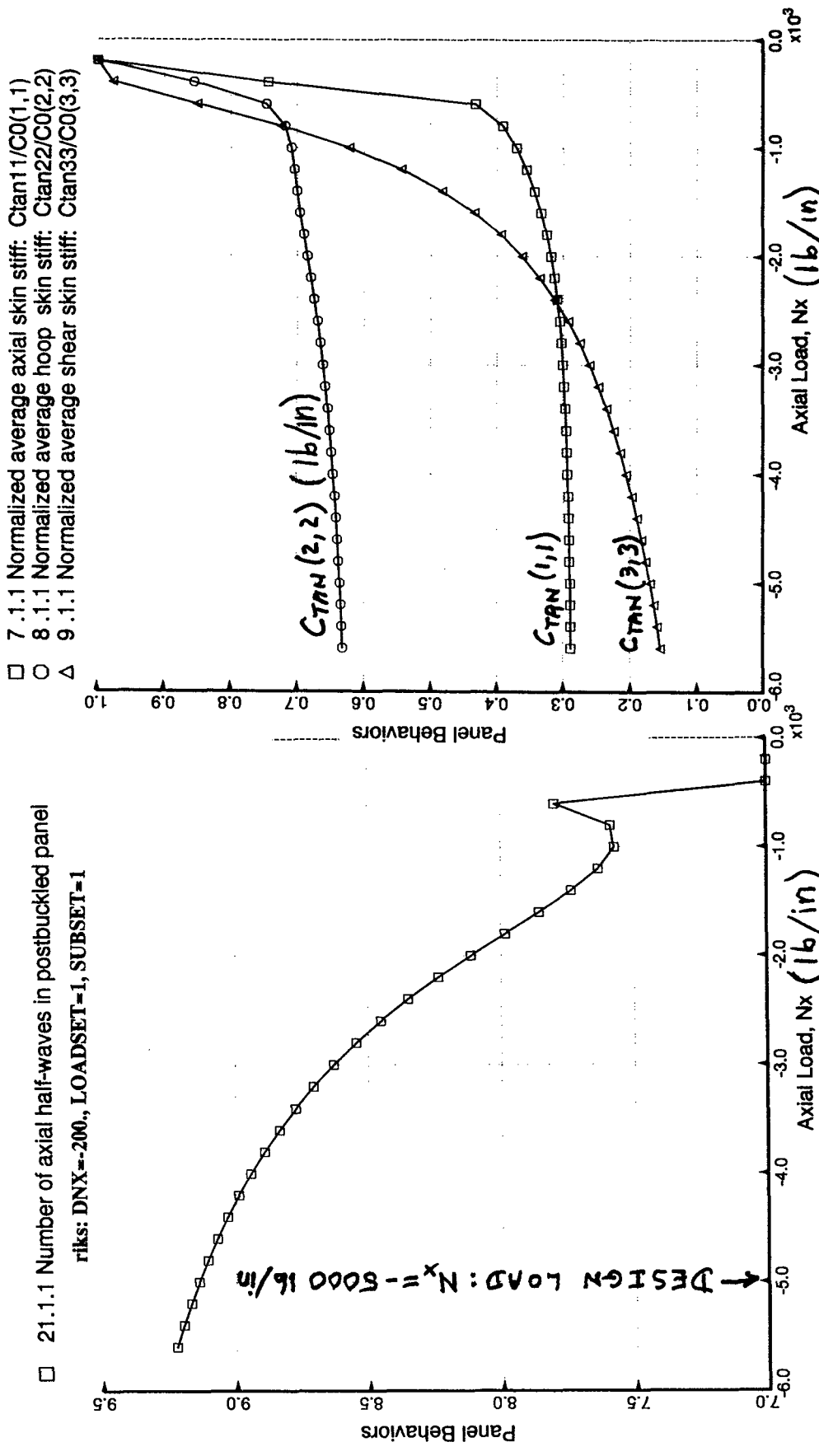

Fig. 8 Theory in PANDA2 [15] accounts for change in the number of axial halfwaves in the locally postbuckled loading regime

Fig. 9 Theory in PANDA2 [19] for wide column and general instability accounts for the change in effective membrane stiffness of a locally postbuckled panel. This is the "classical" long wave and short wave interaction effect.

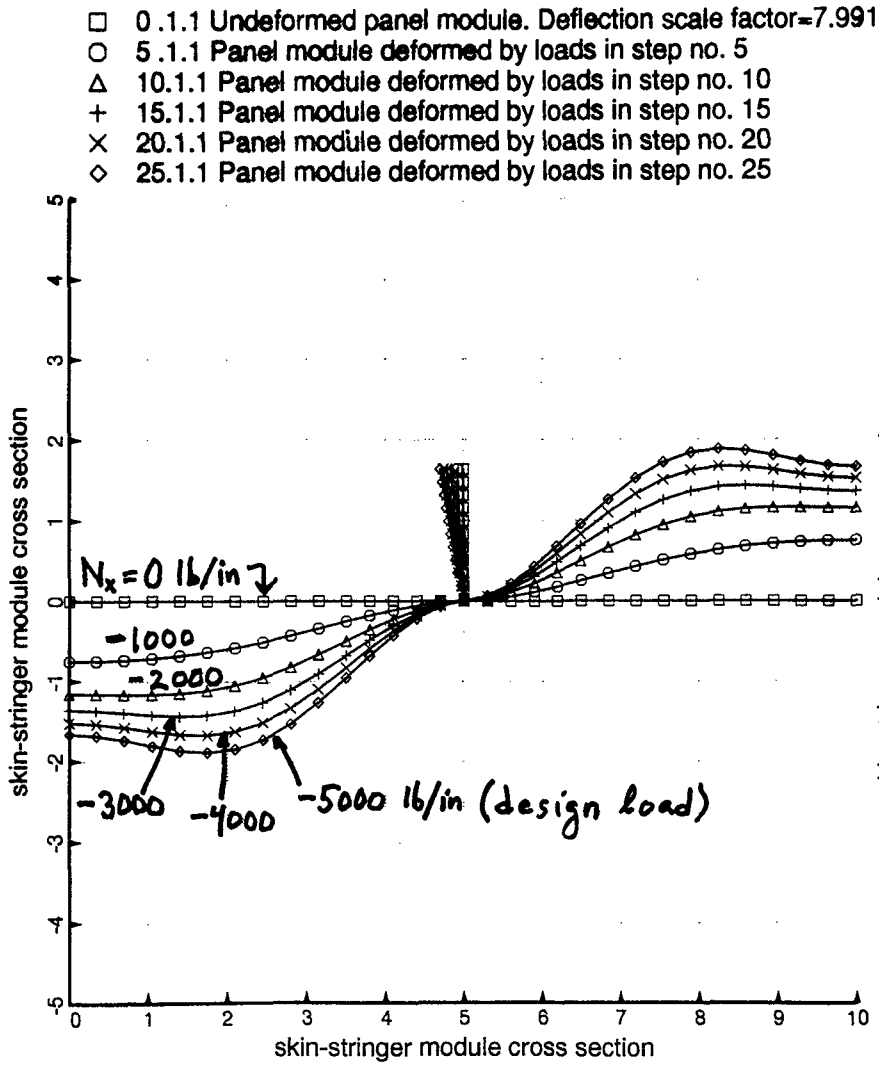

Fig. 10 PANDA2 prediction of locally postbuckled single discretized skin-stringer PANEL I module

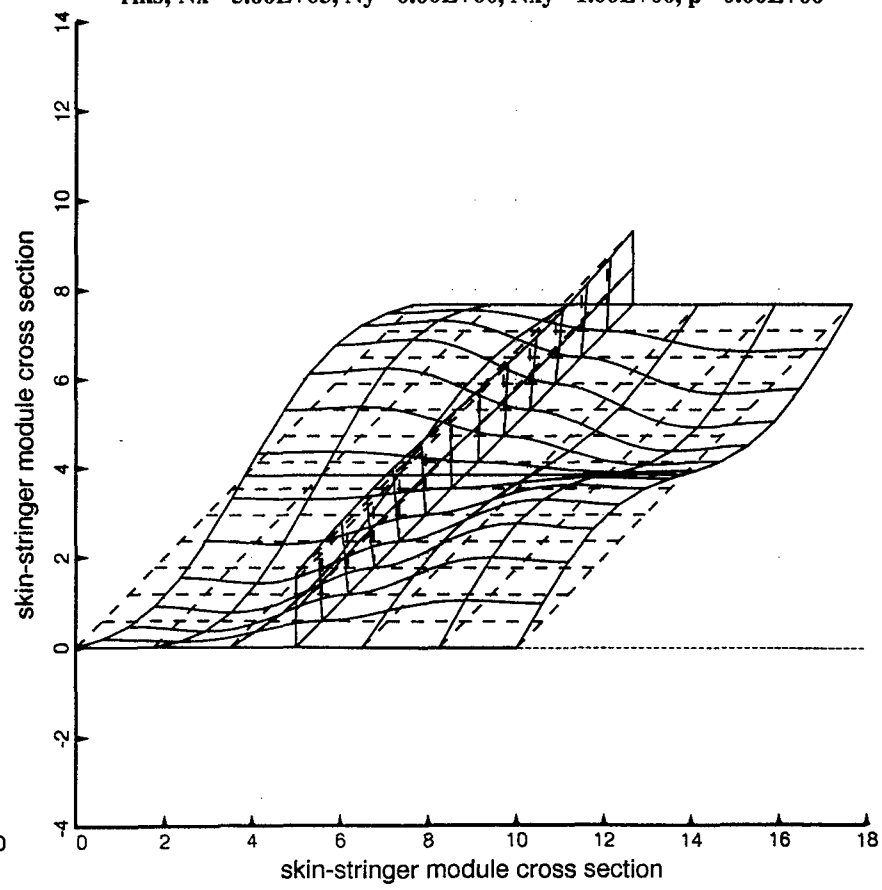

Fig. 11 PANDA2 prediction of locally postbuckled portion of PANEL I of length equal to one full axial wave of the deflection pattern

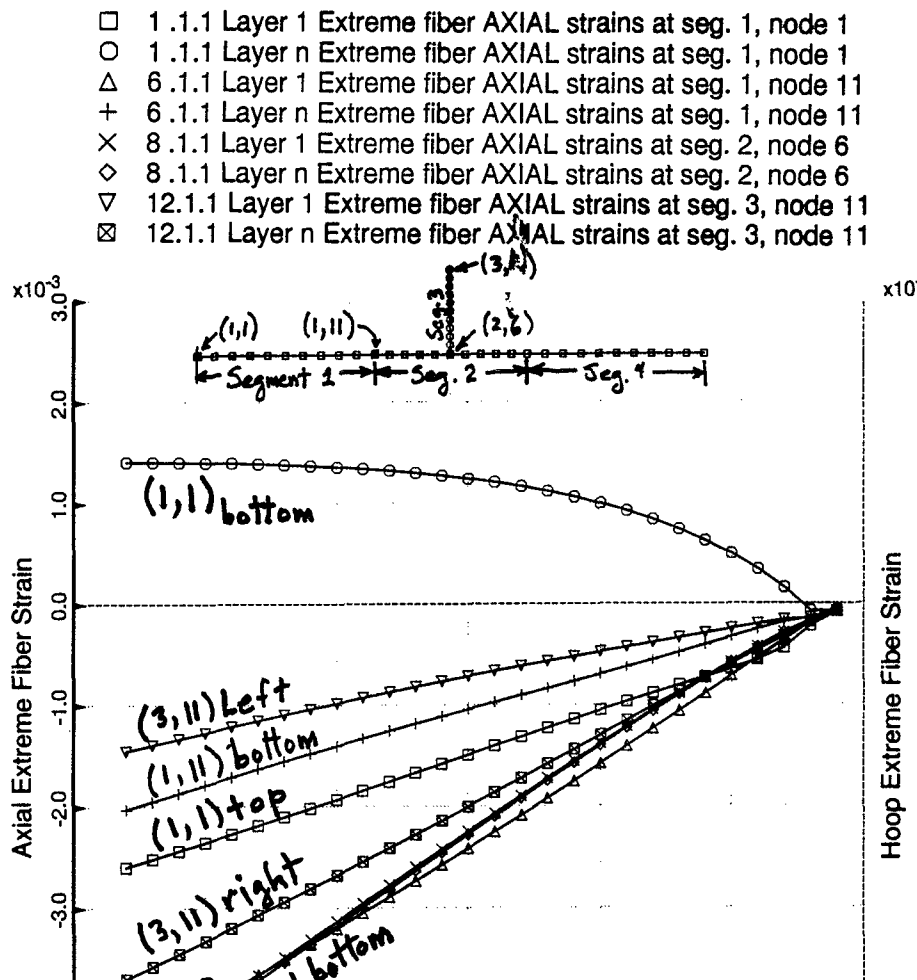

Fig. 12 PANDA2 prediction of axial strain in the surface fibers of the single PANEL I module

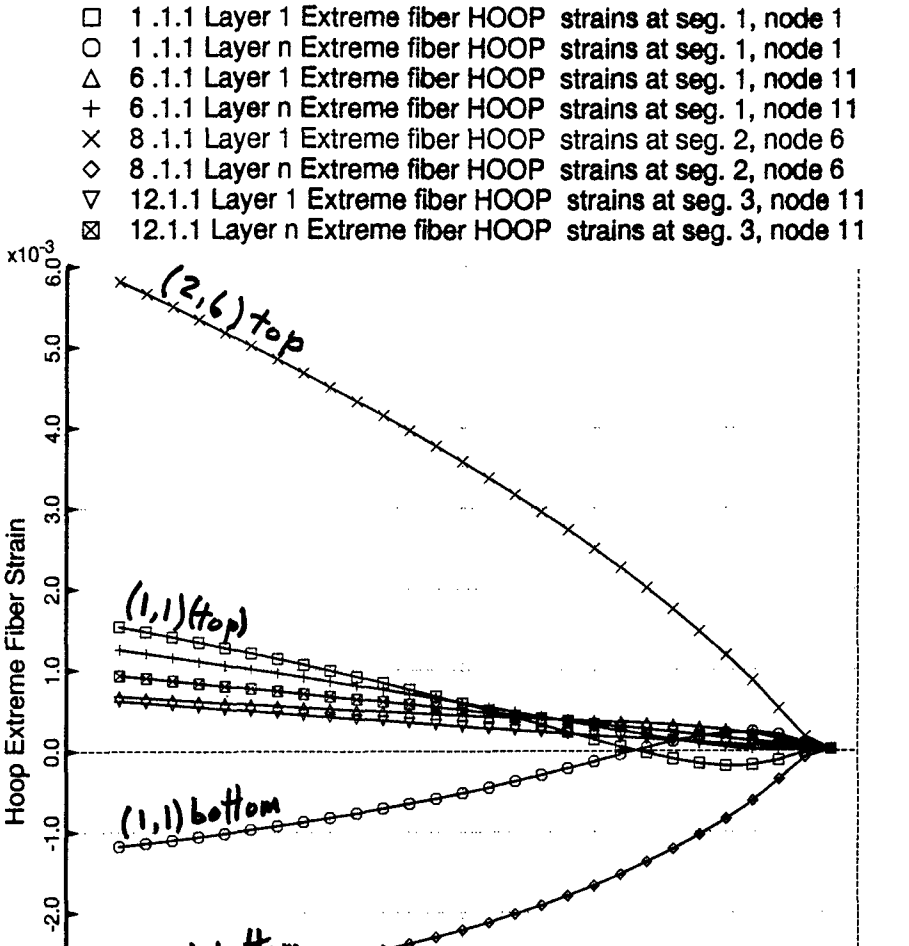

Fig. 13 PANDA2 prediction of hoop strain in the surface fibers of the single PANEL I module

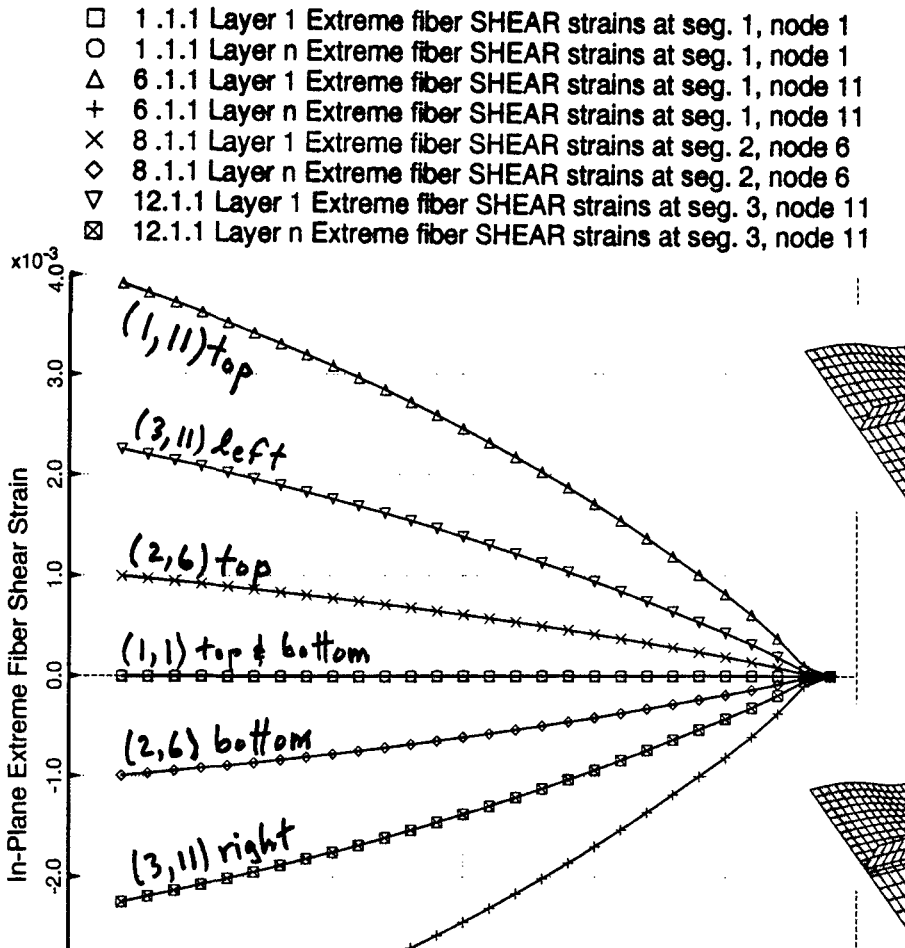

Fig. 14 PANDA2 prediction of in-plane shear strain in the surface fibers of the single PANEL I module

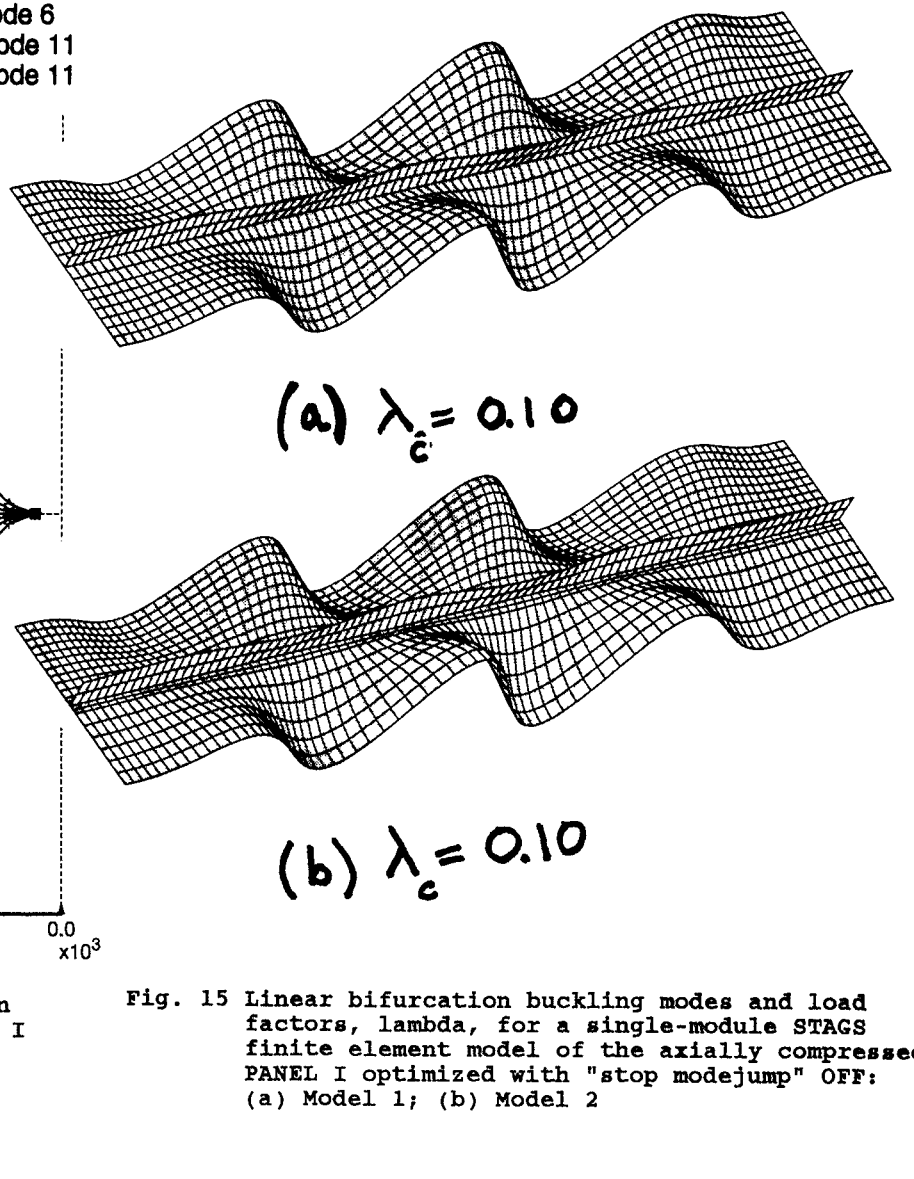

Fig. 15 Linear bifurcation buckling modes and load factors, lambda, for a single-module STAGS finite element model of the axially compressed PANEL I optimized with "stop modejump" OFF: (a) Model 1; (b) Model 2

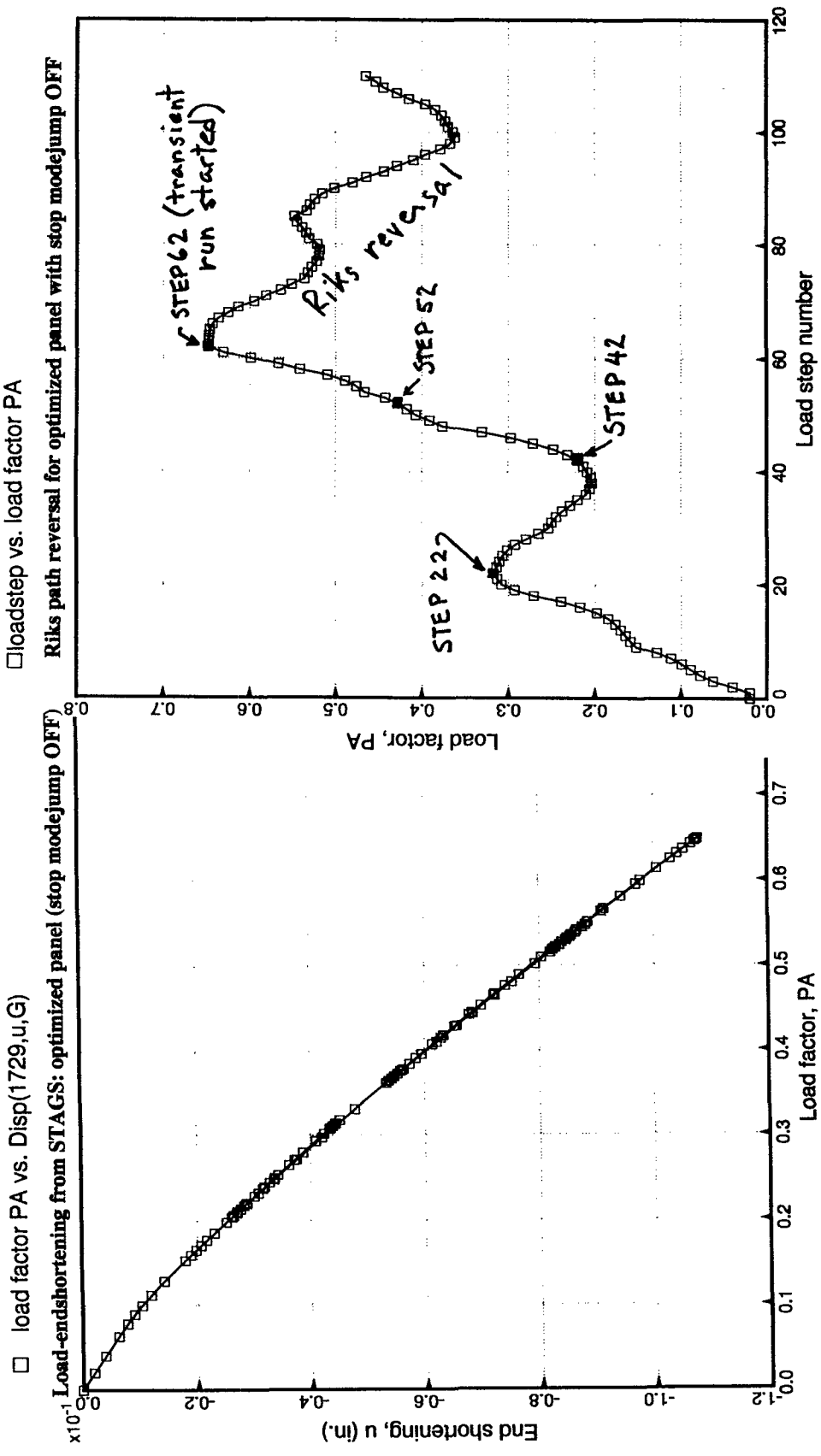

Fig. 16 Load-end-shortening curve for initial STAGS nonlinear static run of PANEL I. STAGS cannot obtain a static solution for a load factor higher than PA = 0.648.

Fig. 17 Loading history showing successful static path-following during initial unloading and unsuccessful "Riks reversal" following attainment of maximum load factor at Step 62

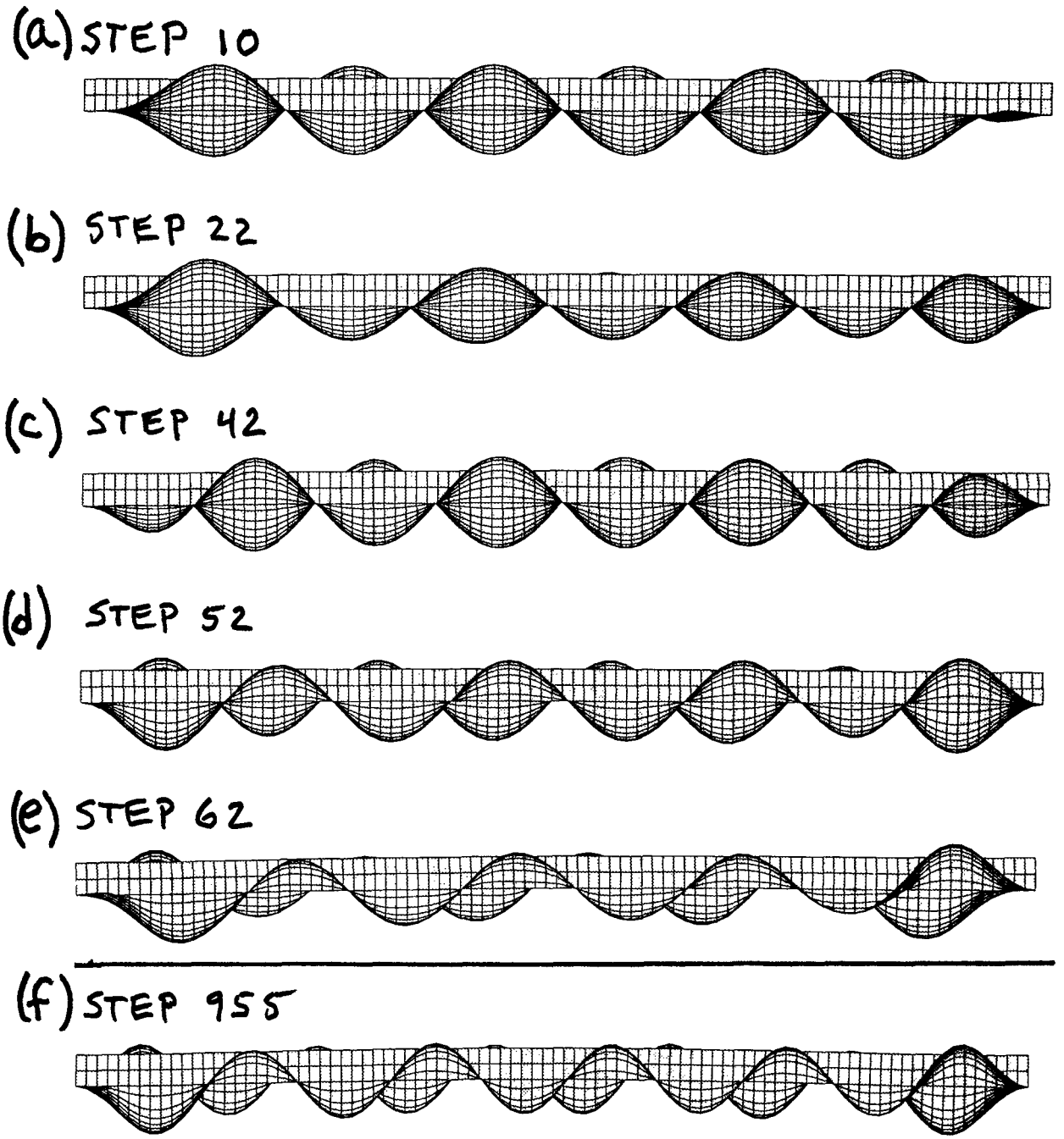

Fig. 18 Edge-on view of locally postbuckled PANEL I showing how the number of axial halfwaves changes during the initial static loading (a)-(e) and after the transient phase (f). The scale factors for deflection are different in each frame so that the maximum amplitudes are the same.

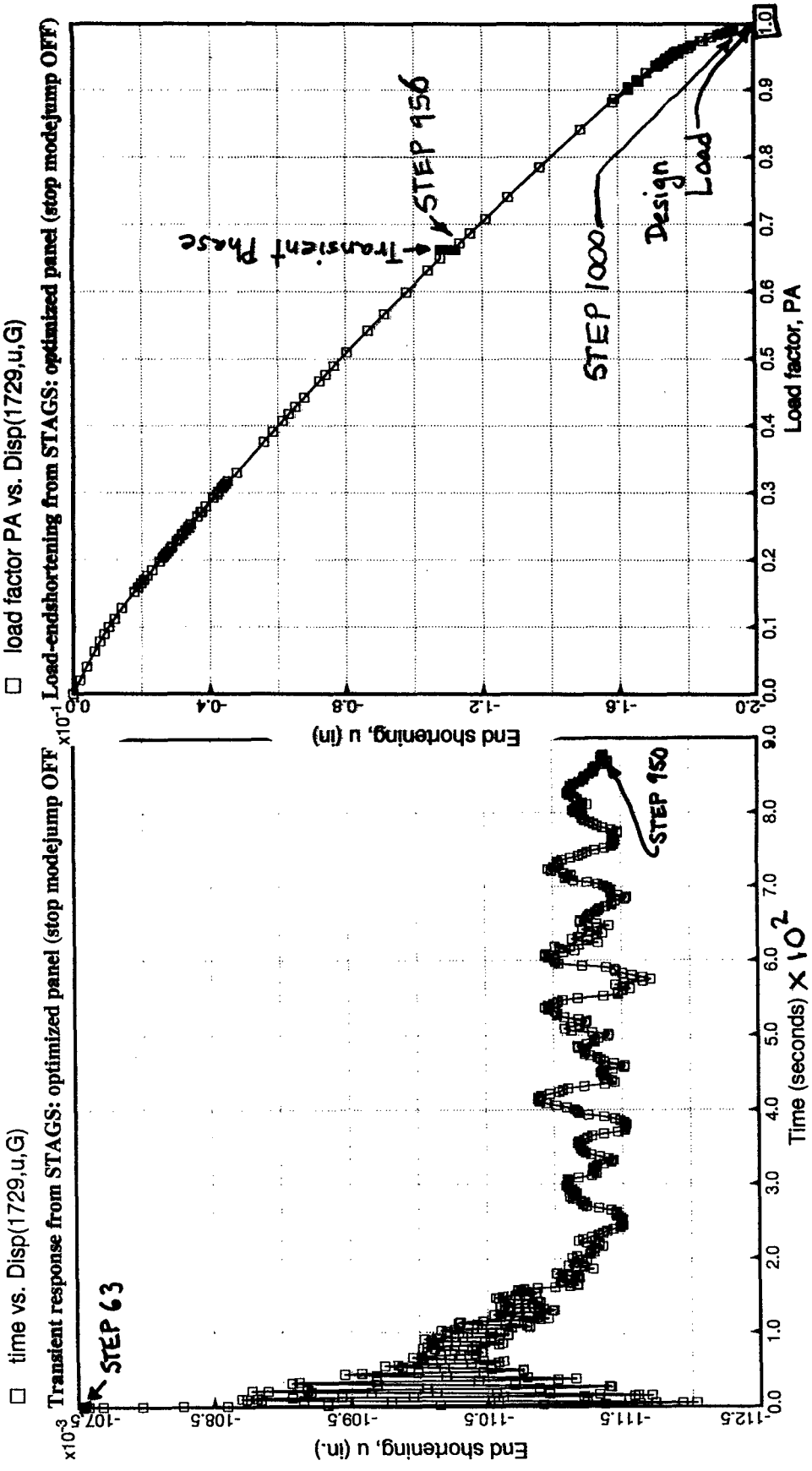

Fig. 19 End shortening during transient phase. The load factor PA is held constant at 0.6605. The maximum time in this frame is 0.09 sec.

Fig. 20 Complete load-end-shortening curve for the STAGS simulation of what happens to PANEL I optimized by PANDA2 with "stop modejump" OFF

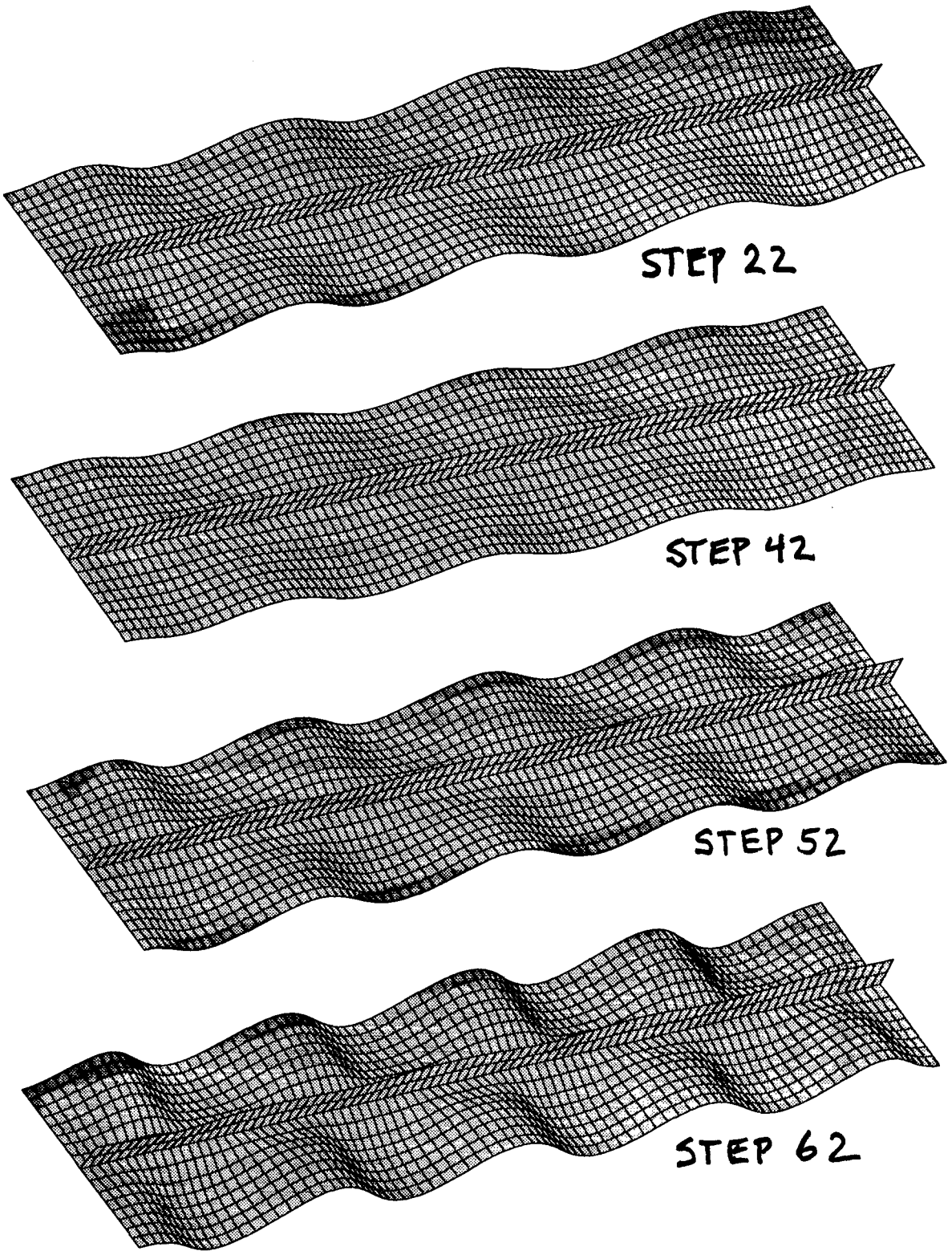

Fig. 21 View of postbuckling deformation of PANEL I during the initial static phase of loading. The same scale factor is used for all frames.

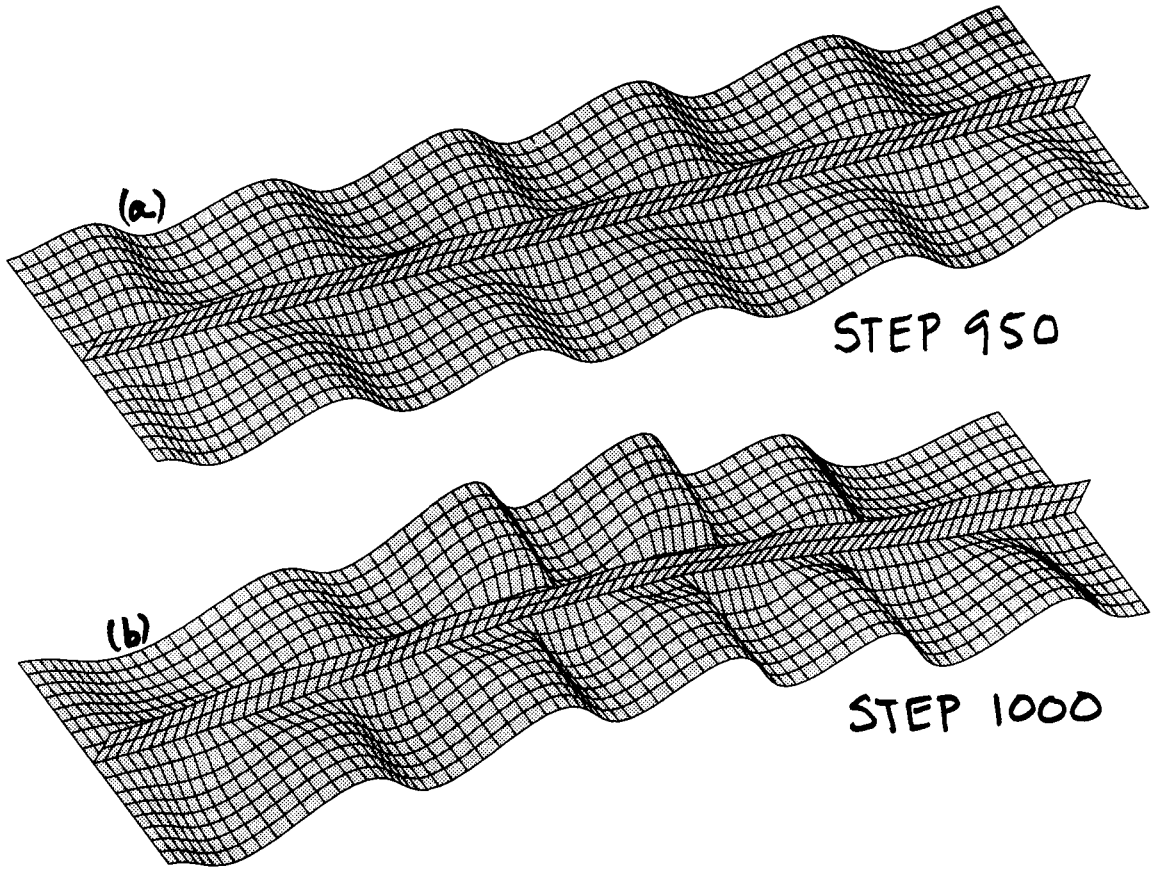

Fig. 22 View of postbuckling deformation of PANEL I at the start and end of the second static phase of loading: 0.660 < PA < 0.991

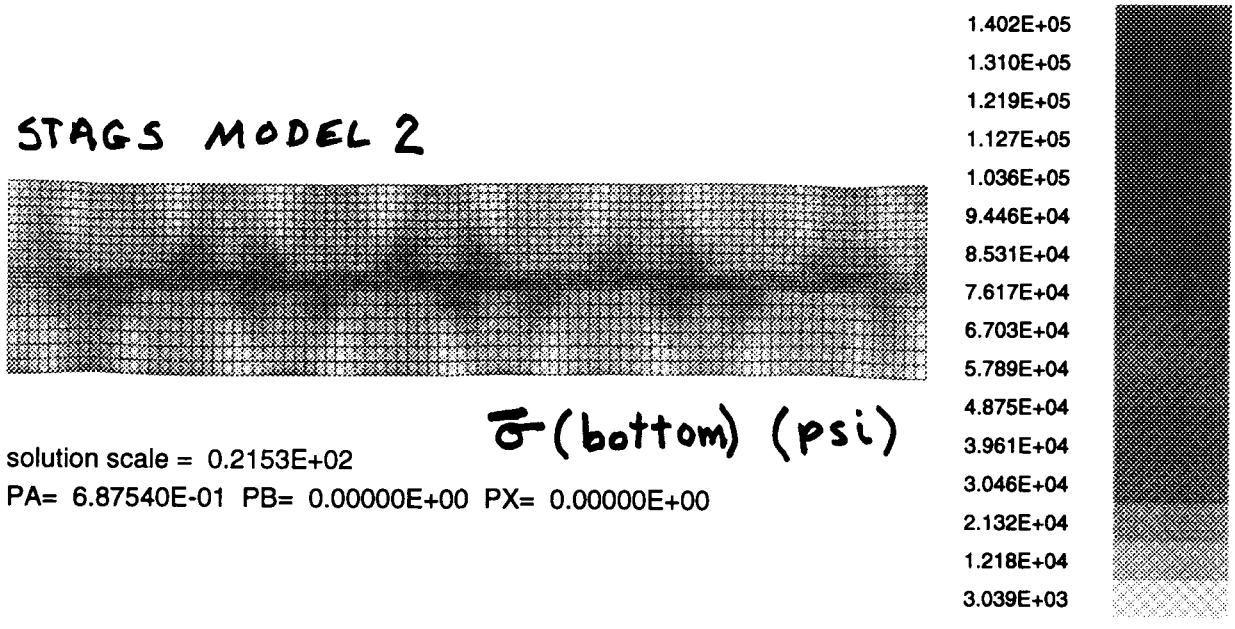

Fig. 23 Effective stress in PANEL I at the skin bottom surface at the load factor, PA = 0.6875, at end of initial static phase for STAGS Finite Element Model 2.

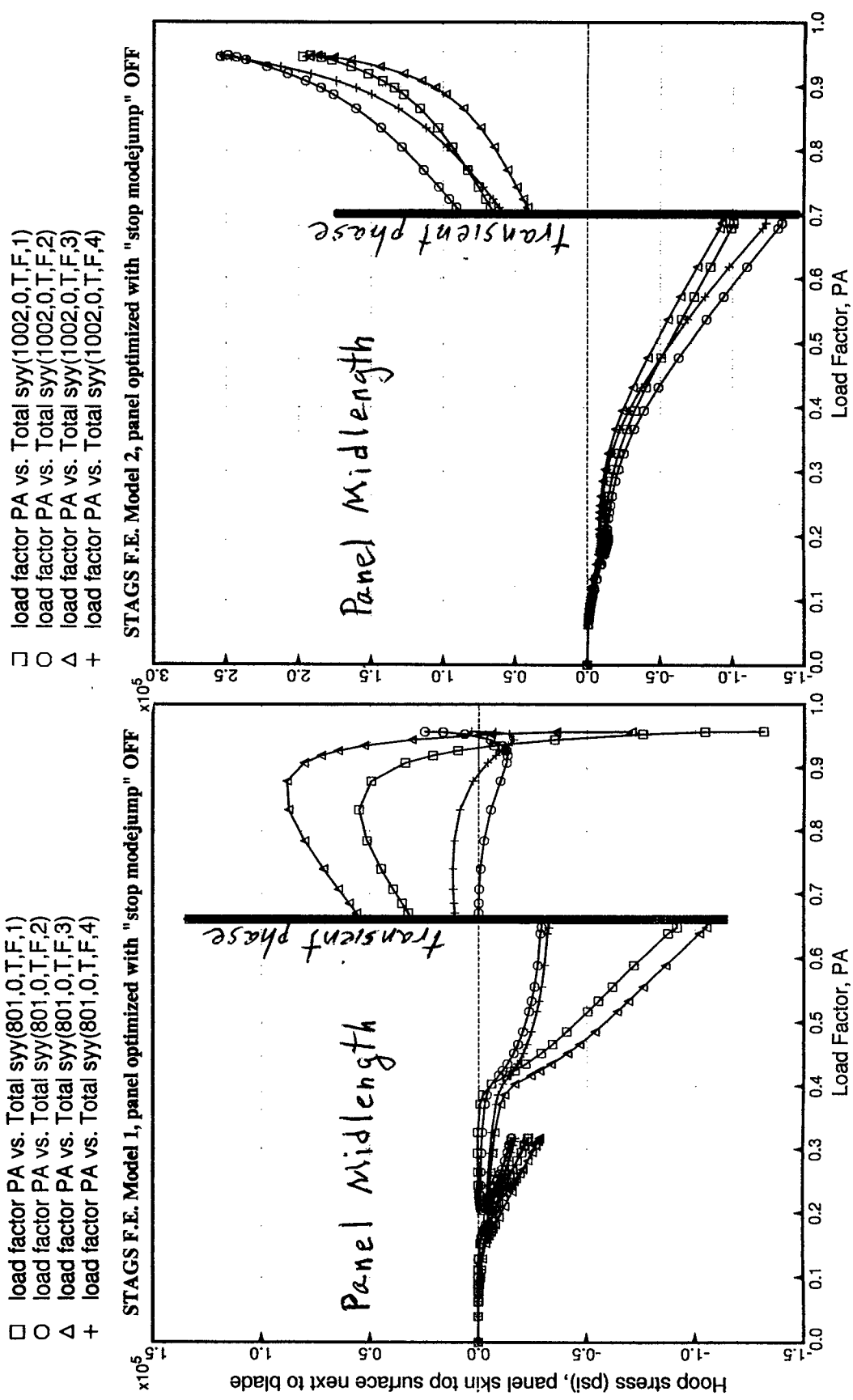

Fig. 24 History of hoop stress in PANEL I at the top surface of the panel skin next to the blade for the "unrefined" finite element Model 1

Fig. 25 History of hoop stress in PANEL I at the top surface of the panel skin next to the blade for the "refined" finite element Model 2

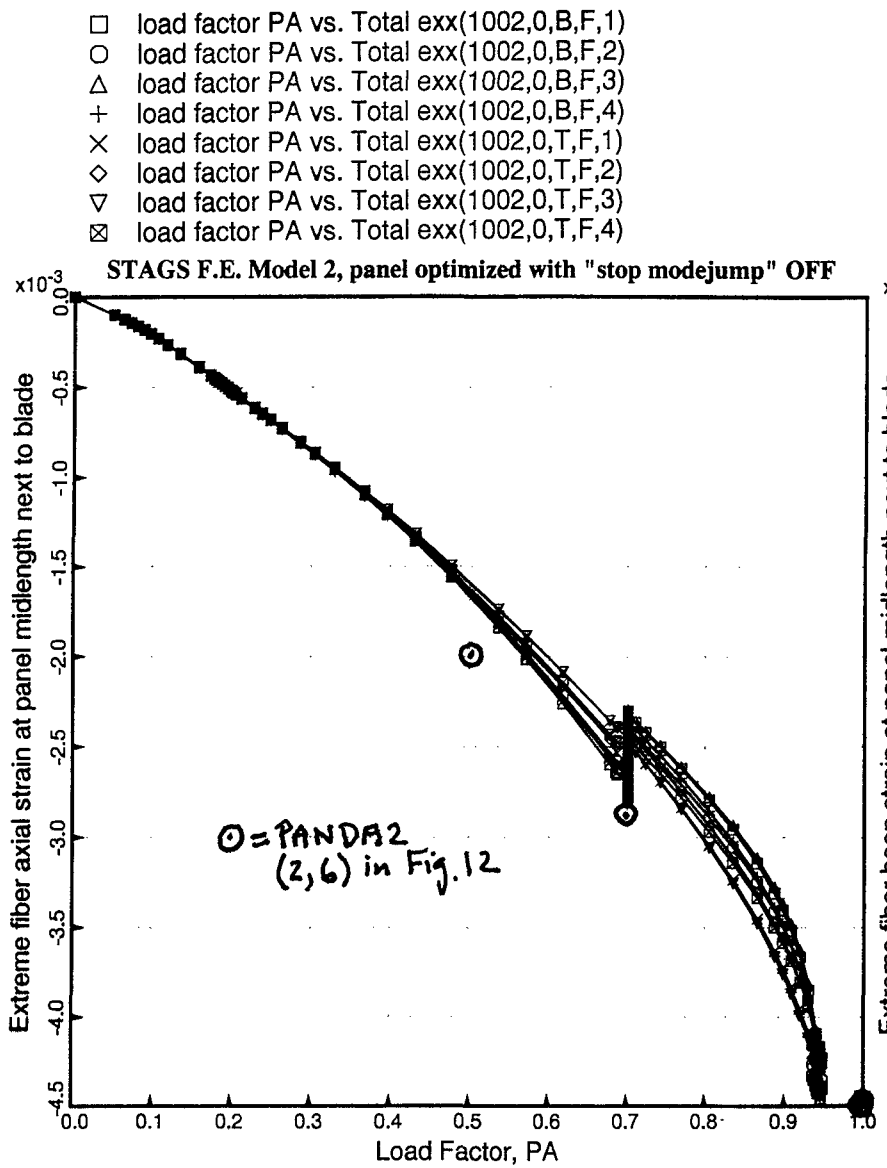

Fig. 26 History of axial strain in PANEL I at the top and bottom surfaces of the panel skin next to the blade. (Compare with Fig. 12)

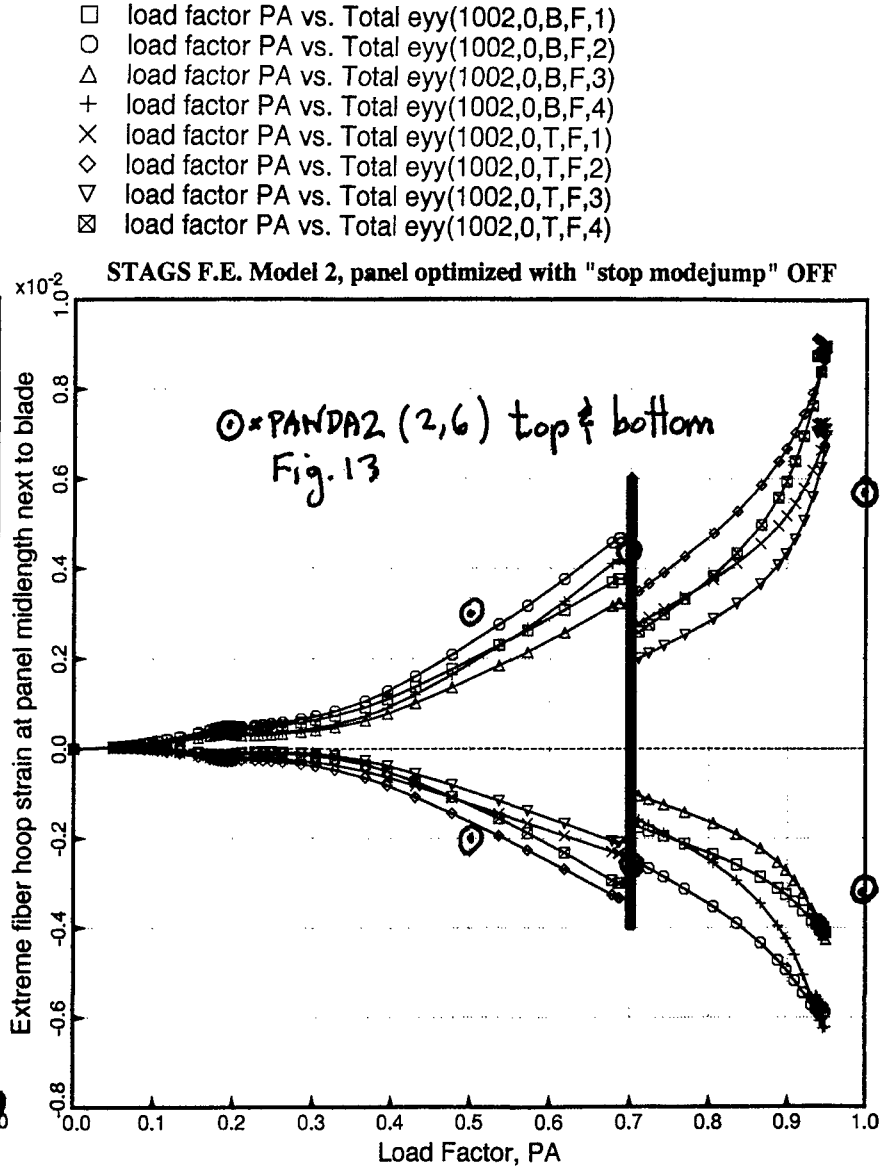

Fig. 27 History of hoop strain in PANEL I at the top and bottom surfaces of the panel skin next to the blade. (Compare with Fig. 13)

Fig. 28 History of shear strain in PANEL I at the top and bottom surfaces of the panel skin next to the blade. (Compare with Fig. 14)

Fig. 29 Edge-on view of postbuckled PANEL I during transient phase at constant load factor PA = 0.7013. Each frame corresponds to a peak value of hoop stress in the next Fig.

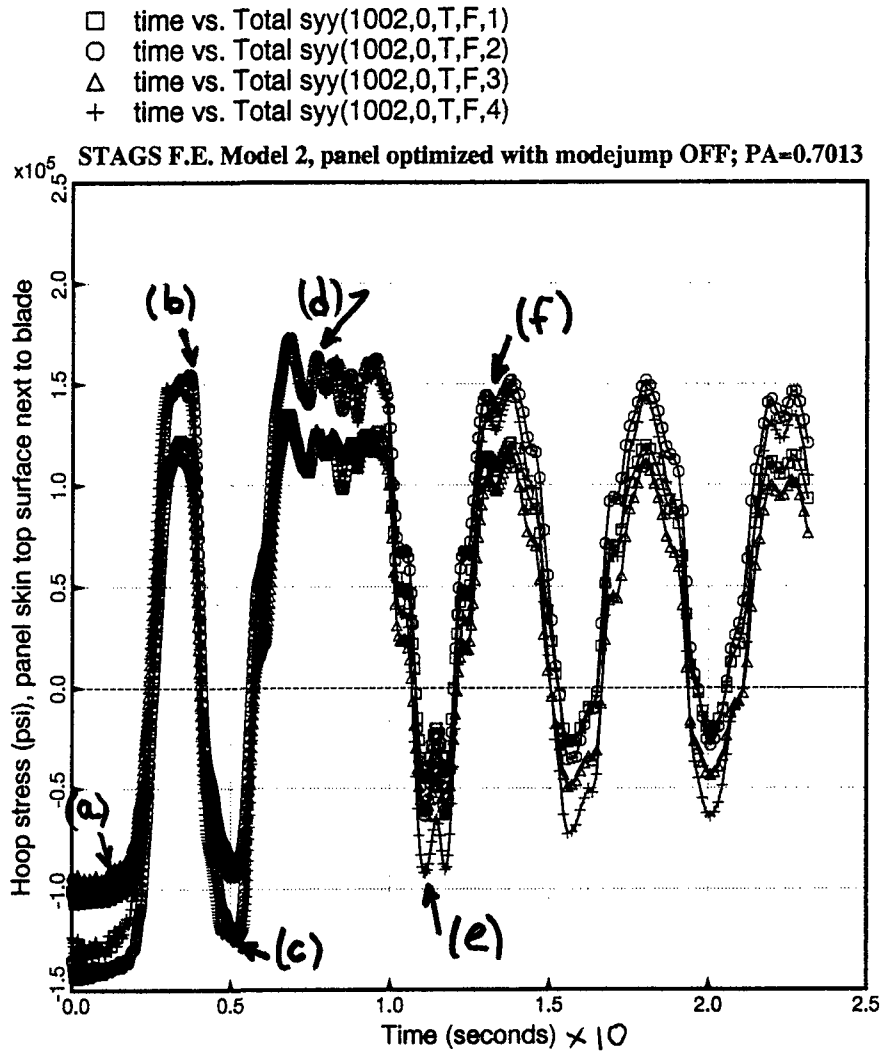

Fig. 30 Oscillations of maximum hoop stress during transient phase (dynamic mode jump). The callouts (a-f) refer to "snapshots" in the previous figure.

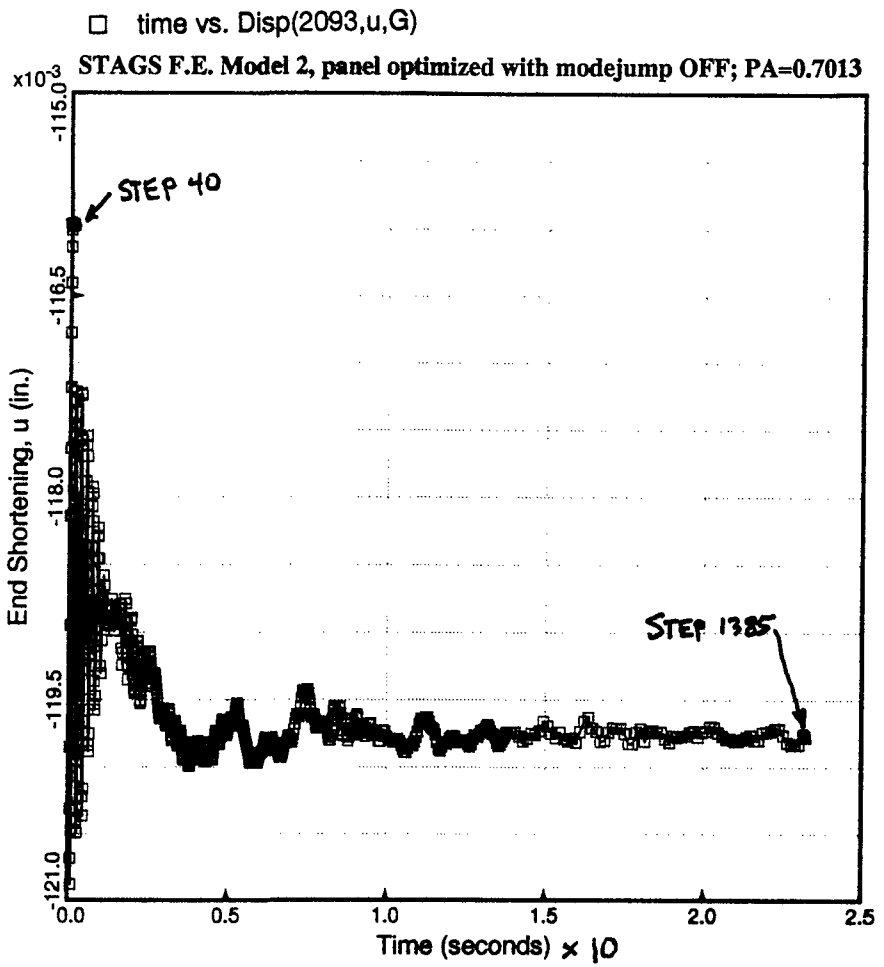

Fig. 31 End shortening during transient phase of PANEL I, Model 2. Although there are only very small changes in end shortening in the range 0.04 < Time < 0.23, there are large oscillations of the maximum hoop stress

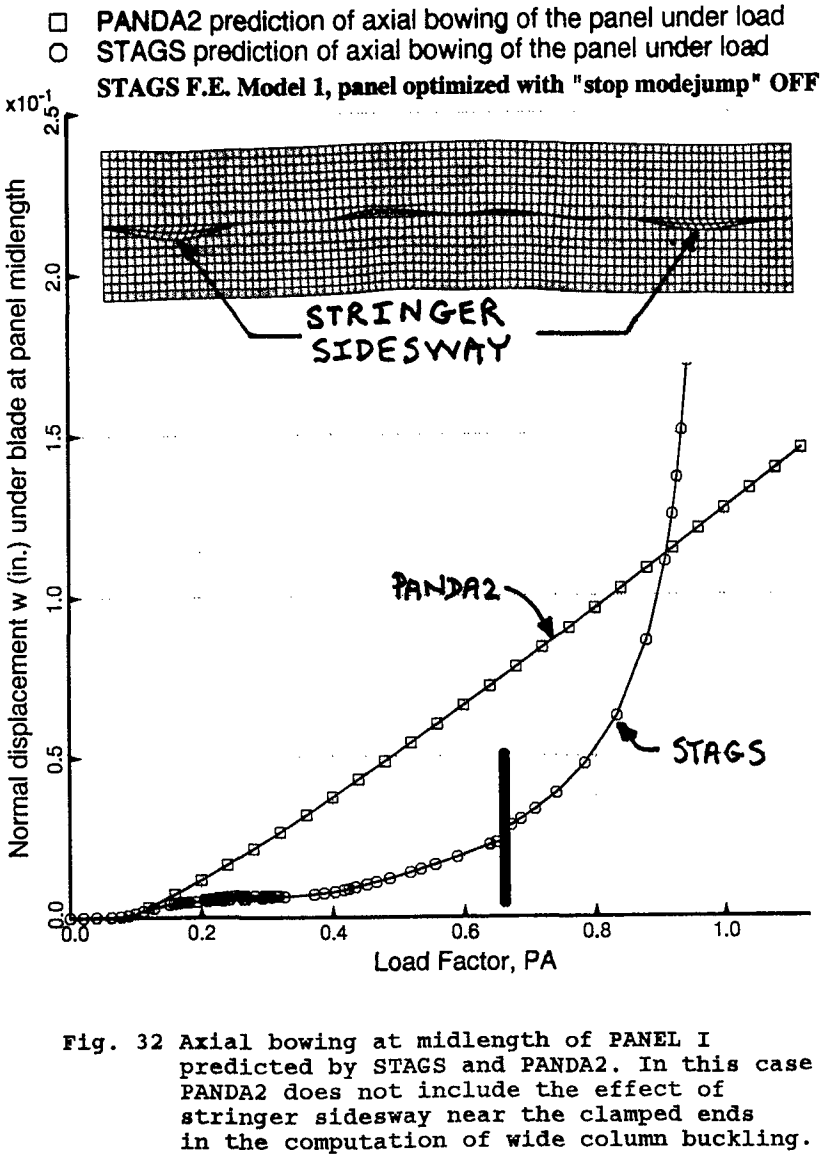

Fig. 32 Axial bowing at midlength of PANEL I predicted by STAGS and PANDA2. In this case PANDA2 does not include the effect of stringer sidesway near the clamped ends in the computation of wide column buckling.

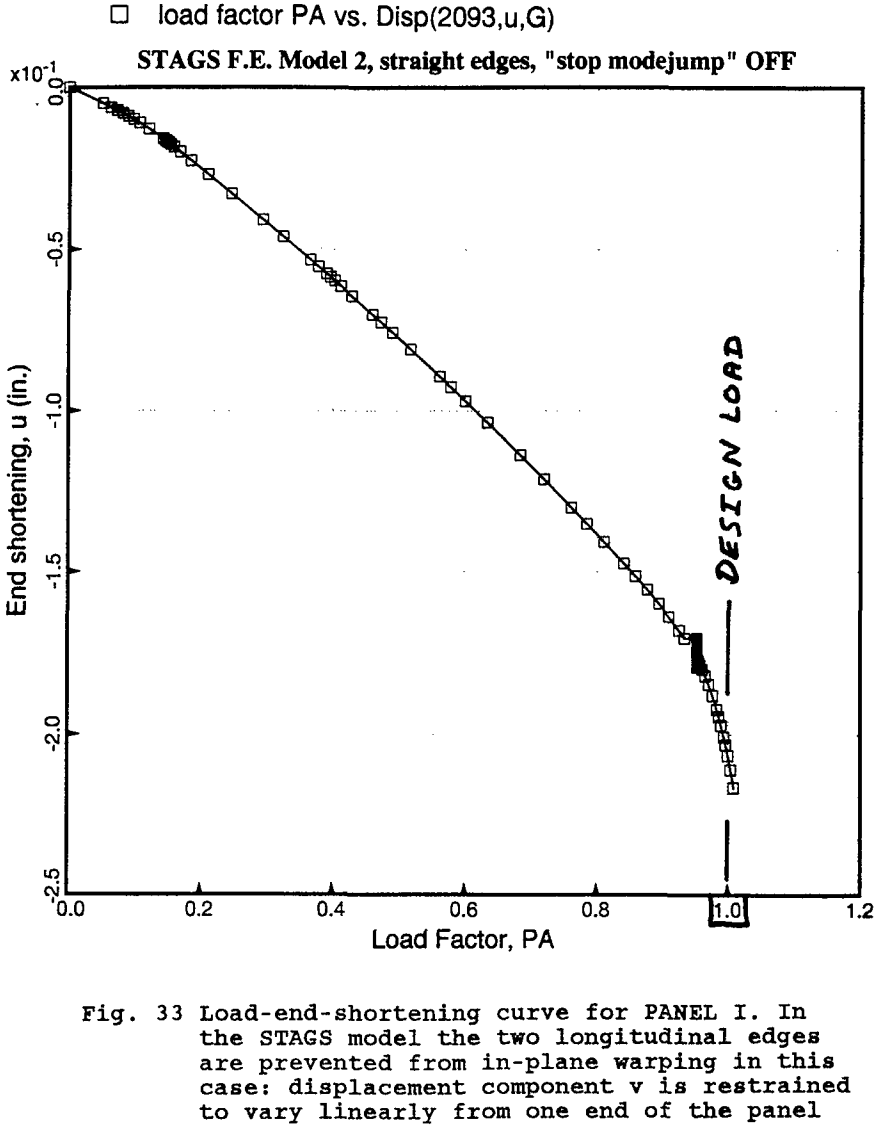

Fig. 33 Load-end-shortening curve for PANEL I. In the STAGS model the two longitudinal edges are prevented from in-plane warping in this case: displacement component v is restrained to vary linearly from one end of the panel to the other.

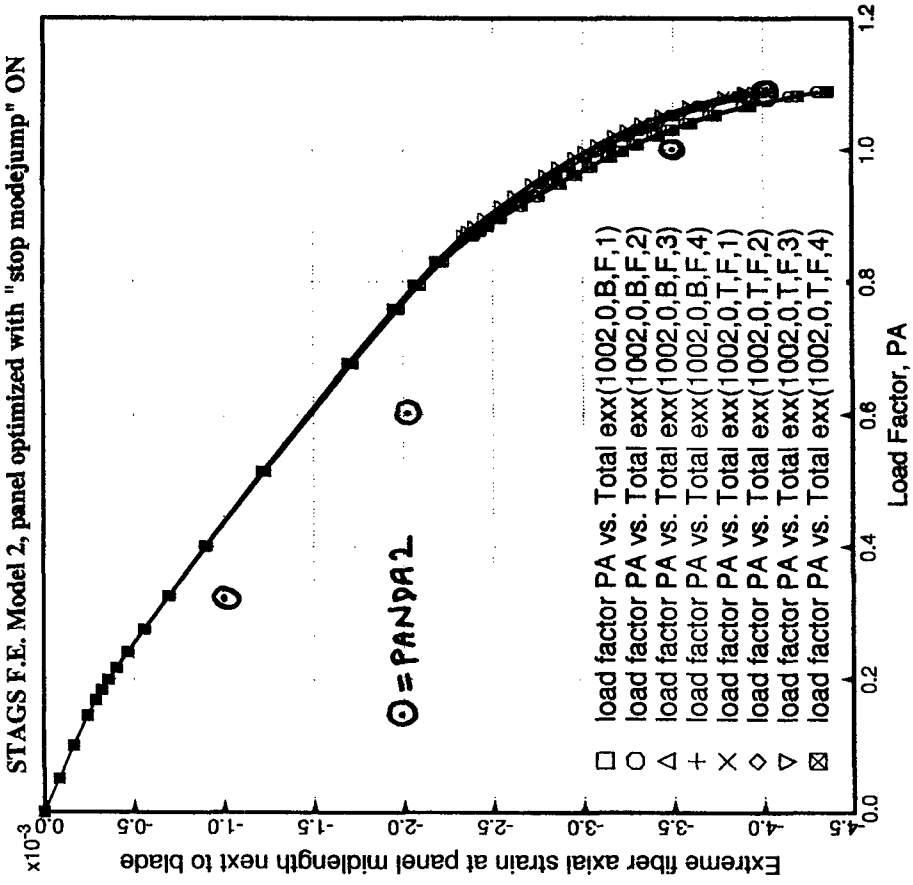

Fig. 35 History of axial strain in PANEL II at the top and bottom surfaces of the panel skin next to the blade.

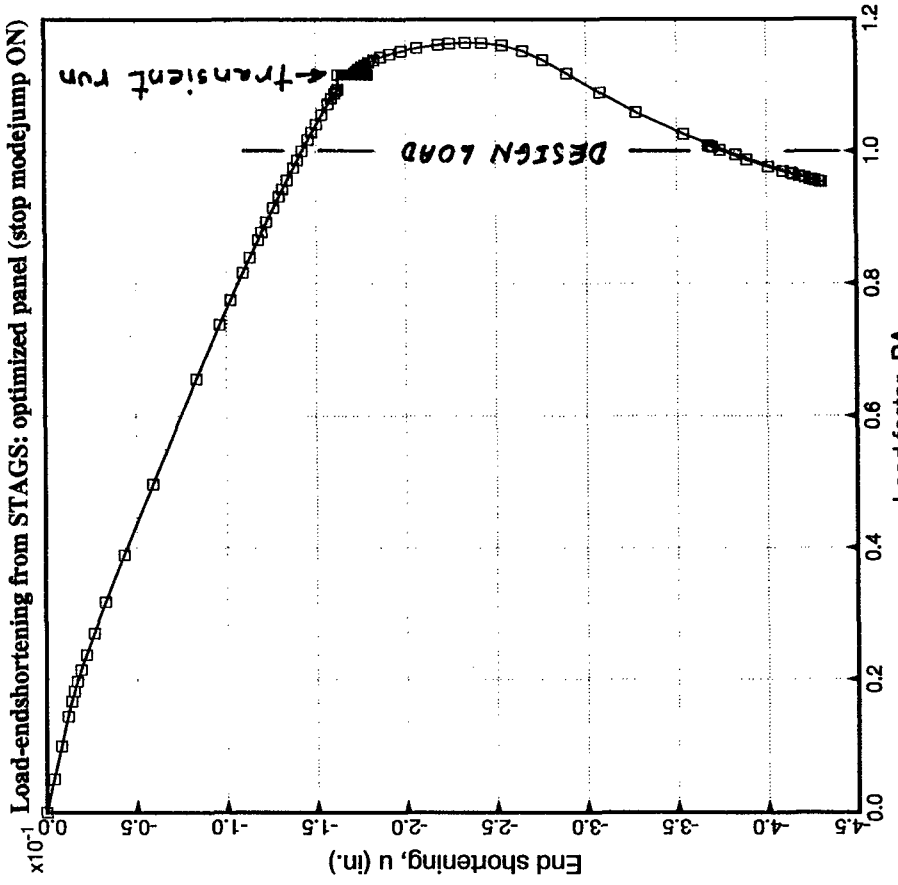

Fig. 34 Load-end-shortening curve for PANEL II, finite element Model 1. PANDA2 predicts mode jumping to occur at the design load.

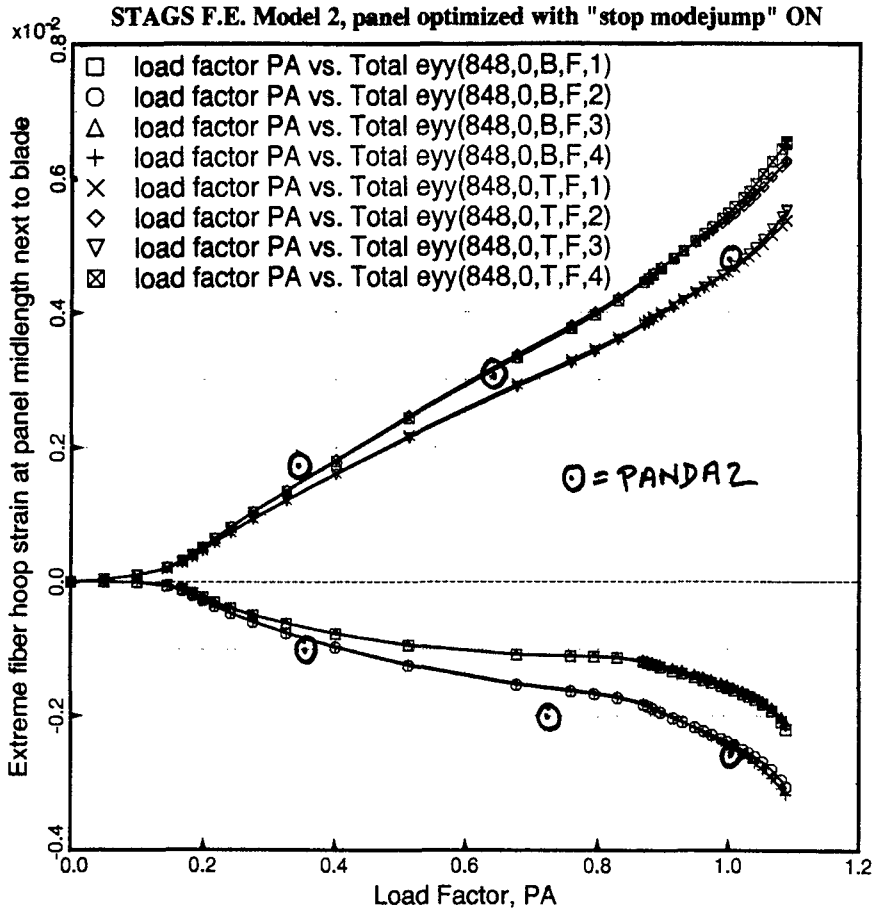

Fig. 36 History of hoop strain in PANEL II at the top and bottom surfaces of the panel skin next to the blade at the location on the axis of the panel where the maximum hoop strain occurs for load factor, PA < 0.6

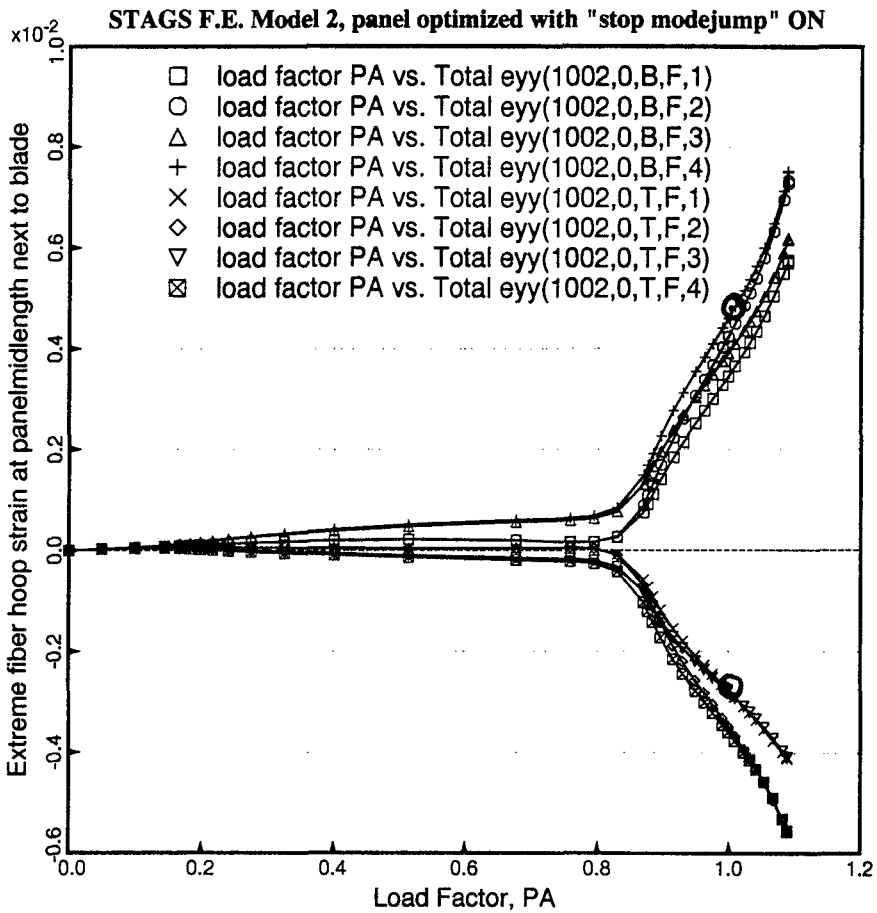

Fig. 37 History of hoop strain in PANEL II at the top and bottom surfaces of the panel skin next to the blade at the location on the axis of the panel where the maximum hoop strain occurs for load factor, PA > 0.9

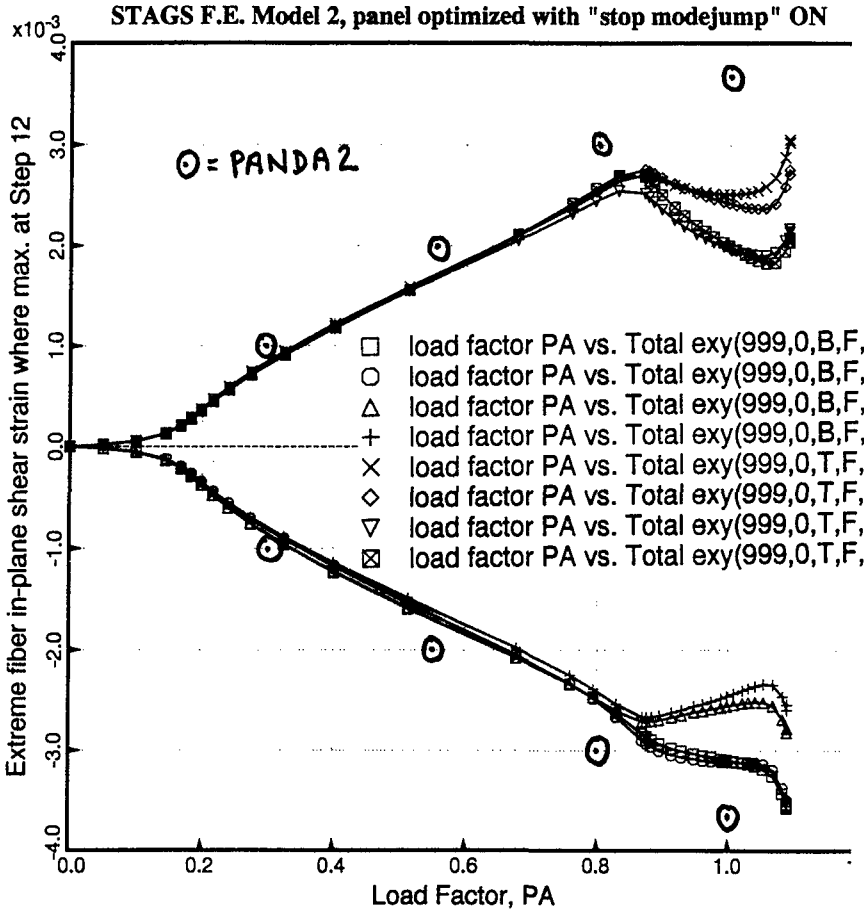

Fig. 38 History of shear strain in PANEL II at the top and bottom surfaces of the panel skin at the location nearest the panel midlength where the maximum shear strain occurs for load factor, PA < 0.6

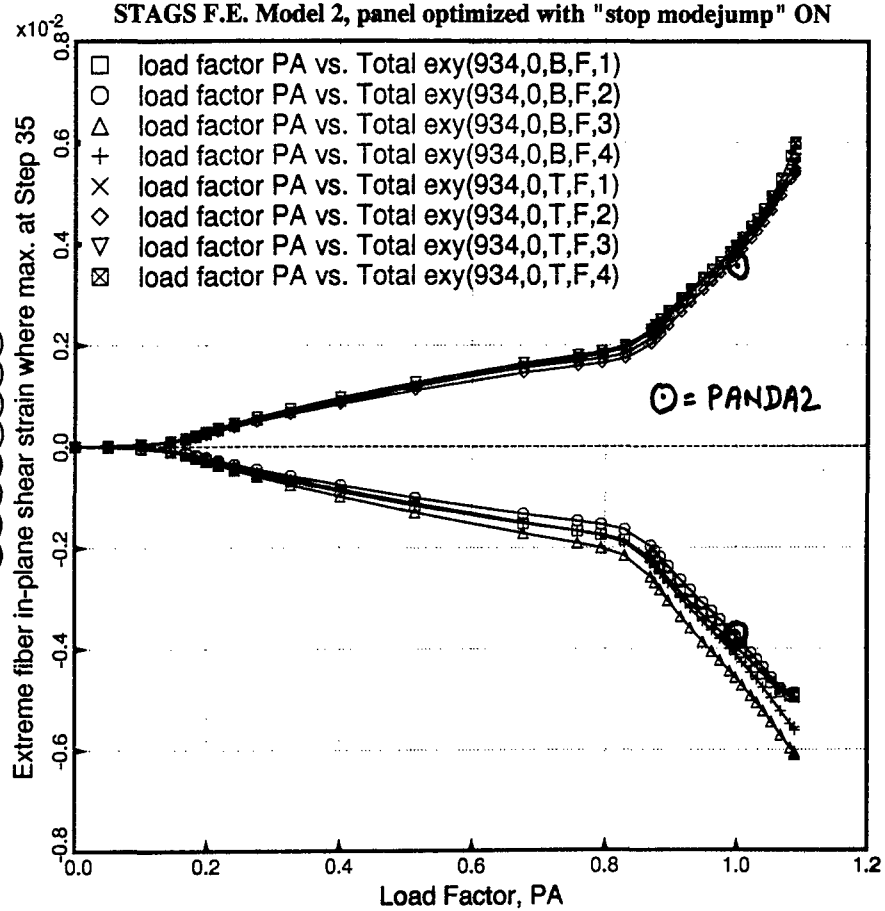

Fig. 39 History of shear strain in PANEL II at the top and bottom surfaces of the panel skin at the location nearest the panel midlength where the maximum shear strain occurs for load factor, PA > 0.9

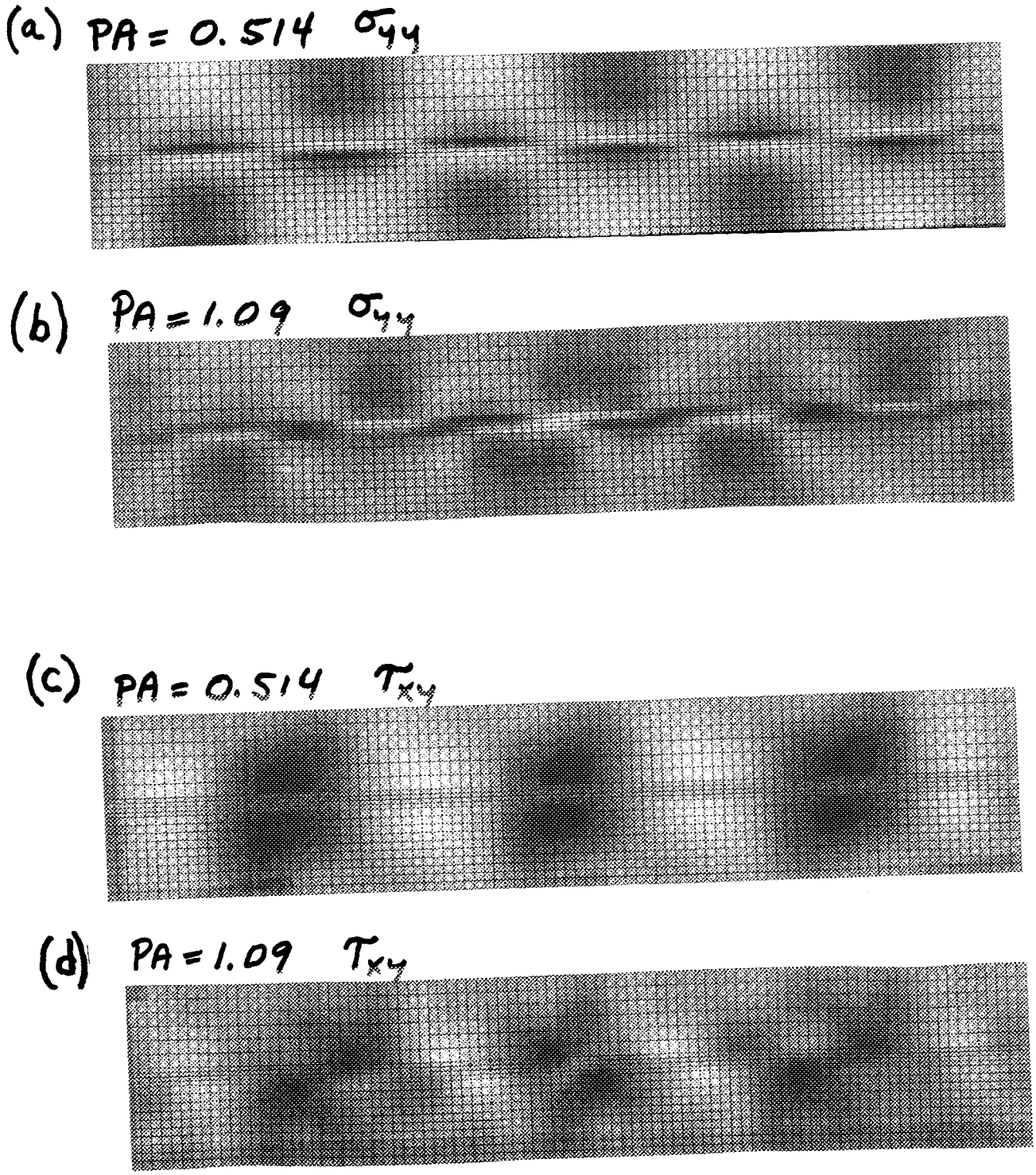

Fig. 40 Fringe plots of (a,b) hoop and (c,d) shear stress at the upper surface in the skin of PANEL II for two load factors. PANDA2 always predicts "in-phase" patterns of the types exhibited in (a) and (c). For load factors near and above the design load (PA=1.0), STAGS predicts relative shifting of the postbuckled lobes on either side of the stringer.